Computer Methods in Applied Mechanics and Engineering 199 (2010) 2456–2471

Contents lists available at ScienceDirect

Computer Methods in Applied Mechanics and Engineering

journal homepage: www.elsevier.com/locate/cma

Stabilized low-order finite elements for frictional contact with the extended finite element method

Fushen Liu, Ronaldo I. Borja *

Department of Civil and Environmental Engineering, Stanford University, Stanford, CA 94305, USA

ARTICLE INFO

Article history:
Received 14 May 2009
Received in revised form 8 December 2009
Accepted 30 March 2010
Available online 9 April 2010

Keywords:
Extended finite element
Frictional contact
Lagrange multipliers
Penalty method
Stabilized methods

ABSTRACT

Contact problem suffers from a numerical instability similar to that encountered in incompressible elasticity, in which the normal contact pressure exhibits spurious oscillation. This oscillation does not go away with mesh refinement, and in some cases it even gets worse as the mesh is refined. Using a Lagrange multipliers formulation we trace this problem to non-satisfaction of the LBB condition associated with equal-order interpolation of slip and normal component of traction. In this paper, we employ a stabilized finite element formulation based on the polynomial pressure projection (PPP) technique, which was used successfully for Stokes equation and for coupled solid-deformation–fluid-diffusion using low-order mixed finite elements. For the frictional contact problem the polynomial pressure projection approach is applied to the normal contact pressure in the framework of the extended finite element method. We use low-order linear triangular elements (tetrahedral elements for 3D) for both slip and normal pressure degrees of freedom, and show the efficacy of the stabilized formulation on a variety of plane strain, plane stress, and three-dimensional problems.

1. Introduction

There exists a large body of literature addressing the computational aspects of contact problems in nonlinear solid mechanics using the finite element (FE) method (see [25,48,51] and references therein). A challenging aspect of the problem is the enforcement of the contact condition, whether it be in the context of classical nonlinear contact mechanics in which element sides are aligned to the contact faces [26,36,37,39,40,42,49,50], or in the framework of the assumed enhanced strain or extended FE method in which contact faces are allowed to pass through and cut the interior of finite elements [2,3,8,11–13,17–20,23,24,27–29,31,34,35,38]. The contact condition inhibits interpenetration of the contact faces, as well as requires that the contact pressure be strictly nonnegative. Mathematically, these constraints are represented by classical Karush–Kuhn–Tucker (KKT) conditions in nonlinear programming, which is a generalization of the method of Lagrange multipliers to inequality constraints. Frictional contact adds complexity to the problem in that a second layer of KKT conditions is necessary to describe stick-slip conditions for the case when the frictional faces are in contact mode [8,19,24,27–29].

The FE method provides a natural tool for simulating frictionless and frictional contact problems. If the contact faces are well defined prior to the beginning of the simulation, then one can simply employ the standard nonlinear contact mechanics approach by aligning element sides with the contact surfaces [25,26,36,37,39,40,42,48–51]. However, if the contact faces are not a priori given and are expected to evolve in an unknown fashion during the course of the simulation, then an extended FE method would be more appropriate [3,4,19,29,33]. The latter approach is generally more robust since it permits the use of instability models [5,9,10,30,41,46] to propagate a discontinuity in any direction and at any point in the solution. In either case, exact satisfaction of the contact constraint may be achieved with a formulation based on the Lagrange multipliers method. Approximate satisfaction of the contact constraint also may be imposed by the penalty method particularly for the more complex problem of frictional sliding.

Irrespective of whether one employs the Lagrange multipliers or penalty method, it is generally recognized that certain combinations of discrete interpolation spaces for solid-displacement and normal contact pressure exhibit numerical instability in the form of spurious oscillation in the normal contact pressure. Typically, these oscillations are more pronounced with the Lagrange multipliers method, where contact constraints are imposed exactly, than with penalty method, where contact constraints are imposed only approximately. Oscillation is somewhat reduced by reducing the values of the penalty parameter, but at the expense of accuracy in the form of significant interpenetration of contact faces. Furthermore, the oscillation does not go away with mesh refinement, and in some cases it even gets worse as the mesh is refined.

Some numerical strategies have been proposed in the literature to address the problem of contact pressure oscillation. Existing stabilized methods include Nitsche's method [38], bubble stabilization [17,18,34], and reduced Lagrange methods [2,24,31]. Bubble

* Corresponding author.
E-mail address: borja@stanford.edu (R.I. Borja).

0045-7825/$ – see front matter © 2010 Elsevier B.V. All rights reserved.
doi:10.1016/j.cma.2010.03.030

stabilization technique introduces additional unknowns, although they can be statically condensed within the element level. It has been shown in [43] that bubble stabilization method is closely related to Nitsche's approach. Unfortunately, the performance of bubble stabilization methods in frictional contact problem has not yet been reported. Mortar method has also been used [24] to address the over-constrained contact problem by reducing the integration points on the interface; however, this approach relies on a heuristic argument for discretizing the interface. In [2,31], a stabilized Lagrange space is designed to satisfy the Ladyzhenskaya–Babuska–Brezzi (LBB) condition [1,14], the basic idea being to reduce the number of Lagrange multipliers by certain rules. However, constructing such a stable Lagrange space is quite complicated, and its FE implementation is not trivial particularly in 3D.

We identify the source of the contact pressure oscillation from failure of the discrete subspaces to satisfy the LBB stability condition similar in spirit to the Stokes problem [21,22,44]. Specifically, certain combinations of discrete subspaces for slip and contact pressure degrees of freedom, particularly those arising from low-order FE interpolations, result in unstable behavior in the form of contact pressure oscillation. Recently, Bochev et al. [6,7,16] quantified the deficiency of some of these low-order mixed finite elements, and proposed a stabilized method aimed at addressing this deficiency. The idea is embodied in so-called polynomial pressure projection (PPP) stabilization, which they used successfully for the Stokes problem. More recently, White and Borja [47] used a similar approach for coupled solid-displacement/fluid-diffusion problem. An analysis of similar pressure projection methods along with a unifying framework for their analysis has also been proposed by Burman [15].

In this paper, we utilize the same PPP technique for stabilizing the frictional contact problem using equal low-order (triangular) interpolations for slip and contact pressure degrees of freedom. Formulation is done with the Lagrange multipliers method for frictionless contact, and with the penalty method for frictional contact. We are not aware of any work in the literature dealing with the implementation of the PPP technique within the framework of the penalty method, and thus, apart from the novel use of this particular technique for the contact problem, we also demonstrate how this technique may be combined with the penalty approach itself. An advantage of the PPP stabilization approach is that the additional stabilizing terms can be assembled locally on each element using standard shape function information, so they introduce minimal additional computational work. Furthermore, the technique is highly suitable for low-order interpolation of displacement and contact pressure fields. To accommodate an evolving slip surface geometry, we implement the stabilized technique in the framework of the extended FE method.

2. Mathematical developments

We consider a classical quasi-static boundary-value problem constrained by the presence of a crack. We denote the problem domain by Ω and enclose it with non-overlapping decompositions of the external boundaries, Γ_{g_i} and Γ_{h_i}, such that

$$\overline{\Gamma_{g_i}\cup\Gamma_{h_i}} = \Gamma, \qquad \Gamma_{g_i}\cap\Gamma_{h_i} = \varnothing, \tag{1}$$

where Γ is the total external boundary and i denotes the ith dimension. We assume that the displacement field g_i is prescribed on Γ_{g_i}, and surface tractions h_i are specified on Γ_{h_i}. In addition, we assume that the body contains an internal crack $\mathcal{S}$ inside a compact support $\Omega^h = \Omega^h_- \cup \Omega^h_+$, with faces $\mathcal{S}_+$ and $\mathcal{S}_-$ interpreted to belong in the "positive" and "negative" sides of the crack, respectively, see Fig. 1. The displacement field $\boldsymbol{u}$ is enhanced to accommodate the crack as follows

$$\boldsymbol{u} = \bar{\boldsymbol{u}} + M_{\mathcal{S}}\tilde{\boldsymbol{u}}, \tag{2}$$

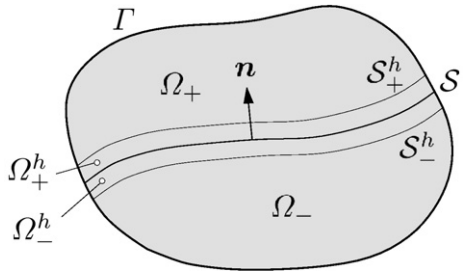

Fig. 1. Domain Ω is cut by a crack $\mathcal{S}$ into Ω_- and Ω_+.

where $\bar{\boldsymbol{u}}$ and $M_{\mathcal{S}}\tilde{\boldsymbol{u}}$ are the continuous and discontinuous parts of displacement, respectively. The scalar function $M_{\mathcal{S}}$ generates the discontinuity on the surface $\mathcal{S}$ and is given by the equation

$$M_{\mathcal{S}} = H_{\mathcal{S}} - f^h, \tag{3}$$

where $H_{\mathcal{S}}$ is the Heaviside function defined by

$$H_{\mathcal{S}} = \begin{cases} 1, & \boldsymbol{x}\in\Omega_+ \\ 0, & \boldsymbol{x}\in\Omega_- \end{cases}, \tag{4}$$

and $f^h(\boldsymbol{x})$ is any arbitrary smooth function that satisfies the requirements $f^h = 0$ in $\Omega_-\backslash\Omega^h_-$, and $f = 1$ in $\Omega_+\backslash\Omega^h_+$. The jump of $M_{\mathcal{S}}$ on $\mathcal{S}$ is $[\![M_{\mathcal{S}}]\!] = 1$, and $M_{\mathcal{S}} = 0$ on the surface $\mathcal{S}^h_\pm$.

The strong form of the boundary-value problem is as follows. For all $\boldsymbol{x}\in\Omega$, find the admissible displacement field $\boldsymbol{u}$ such that

$$\boldsymbol{\nabla}\cdot\boldsymbol{\sigma} + \boldsymbol{f} = \boldsymbol{0} \qquad \text{in } \Omega\backslash\mathcal{S} \tag{5}$$

$$u_i = g_i \qquad \text{on } \Gamma_{g_i} \tag{6}$$

$$(\boldsymbol{\nu}\cdot\boldsymbol{\sigma})_i = h_i \qquad \text{on } \Gamma_{h_i} \tag{7}$$

$$\boldsymbol{n}\cdot\boldsymbol{\sigma} = \boldsymbol{t}_- \qquad \text{on } \mathcal{S}_- \tag{8}$$

$$-\boldsymbol{n}\cdot\boldsymbol{\sigma} = \boldsymbol{t}_+ \qquad \text{on } \mathcal{S}_+, \tag{9}$$

where $\boldsymbol{\sigma}$ is the Cauchy stress tensor (a function of the symmetric gradient of the displacement field, $\boldsymbol{\nabla}^s\boldsymbol{u}$), $\boldsymbol{f}$ is the body force vector, $\boldsymbol{\nu}$ is the unit outward normal vector to Γ_{h_i}, and $\boldsymbol{n}$ is the unit outward normal vector to $\mathcal{S}_-$. Traction boundary conditions on the crack faces demands that $\boldsymbol{t}_+ = -\boldsymbol{t}_-$.

We next impose the contact condition. Let the gap between $\mathcal{S}_-$ and $\mathcal{S}_+$ be denoted by

$$h(\boldsymbol{x}) = (\boldsymbol{u}_+ - \boldsymbol{u}_-)\cdot\boldsymbol{n} = \tilde{\boldsymbol{u}}\cdot\boldsymbol{n}, \qquad \boldsymbol{x}\in\mathcal{S}. \tag{10}$$

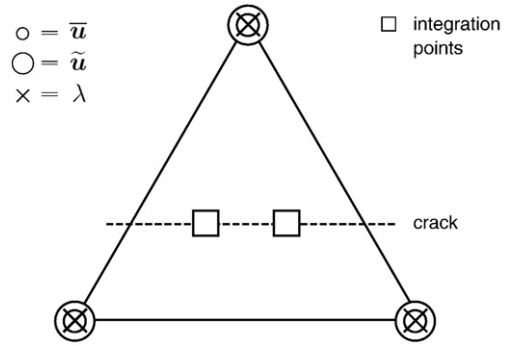

Fig. 2. Enriched CST element crossed by a crack. Each node has $\bar{\boldsymbol{u}}$, $\tilde{\boldsymbol{u}}$, and λ degrees of freedom.

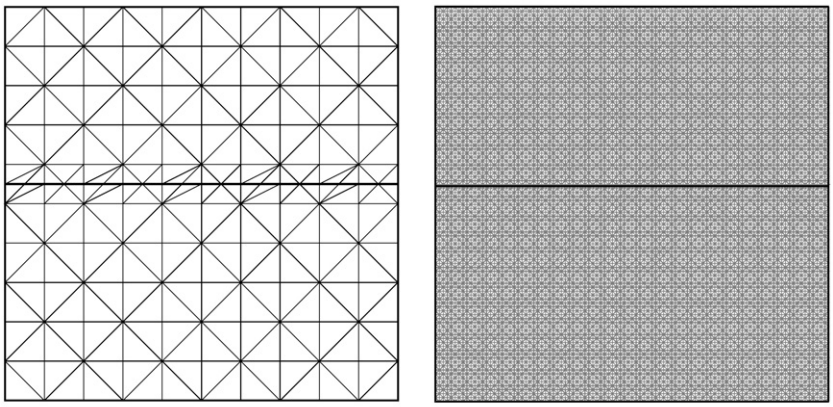

Fig. 3. Structured FE meshes for simulations with frictionless contact: Mesh 1 has 121 nodes and 200 CST elements. Mesh 2 has 10,201 nodes and 20,000 CST elements. Sub-triangles around the crack are used for numerical integration only, and do not define additional CST elements.

Further, let the normal contact pressure be denoted by $\lambda(\boldsymbol{x})$. The constraint introduced by the presence of the crack is given in compact form by the KKT conditions

$$\lambda(\boldsymbol{x})\geq 0, \qquad -h(\boldsymbol{x})\leq 0, \qquad \lambda(\boldsymbol{x})h(\boldsymbol{x}) = 0, \qquad \forall \boldsymbol{x}\in\mathcal{S}. \tag{11}$$

In other words, the normal contact pressure $\lambda(\boldsymbol{x})$ must be positive whenever $h(\boldsymbol{x})=0$, and is zero whenever $-h(\boldsymbol{x})<0$.

To develop the weak form, we consider a set of trial functions

$$\mathcal{U}_i = \left\{u_i \,|\, u_i \in H^1(\Omega), u_i = g_i \text{ on } \Gamma_{g_i}\right\} \tag{12}$$

and a set of variations

$$\mathcal{V}_i = \left\{\eta_i \,|\, \eta_i \in H^1(\Omega), \eta_i = 0 \text{ on } \Gamma_{g_i}\right\}. \tag{13}$$

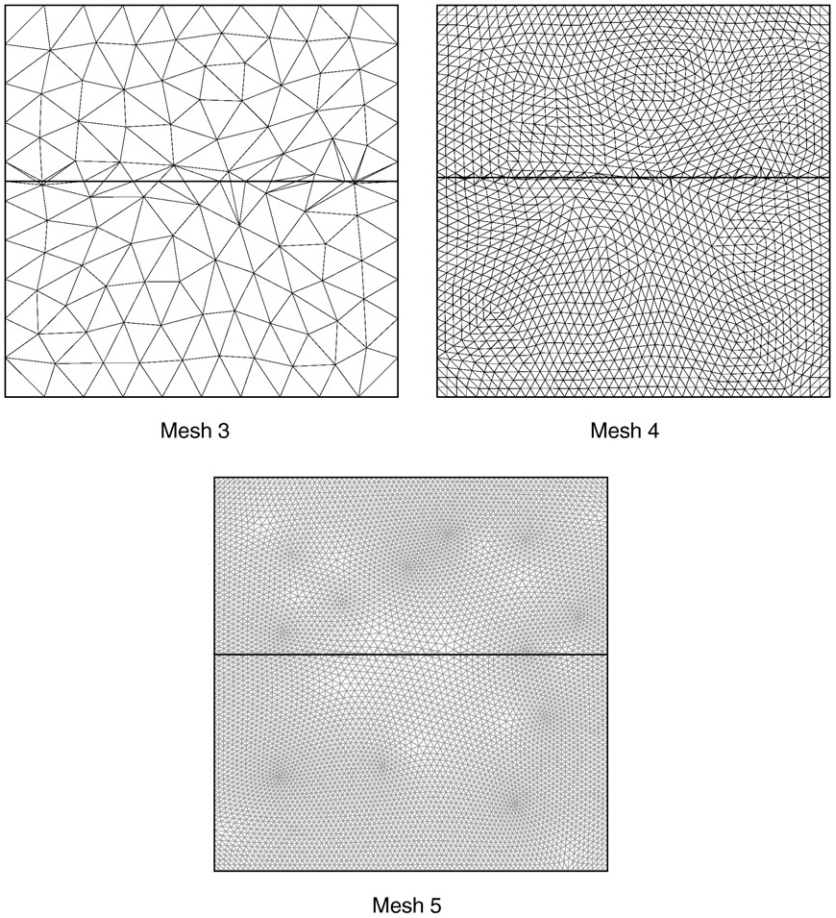

Fig. 4. Unstructured FE meshes for simulations with frictionless contact: Mesh 3 has 121 nodes and 200 CST elements; Mesh 4 has 1681 nodes and 3200 CST elements; Mesh 5 has 6561 nodes and 12,800 CST elements.

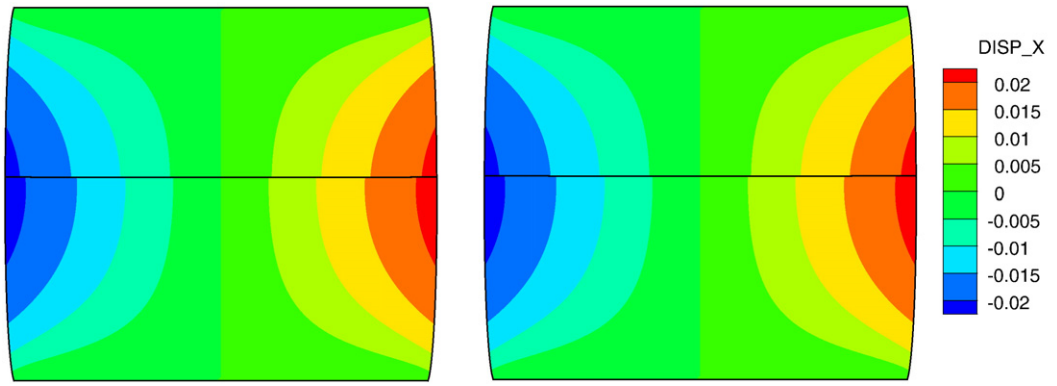

Fig. 5. Contours of horizontal displacements using Mesh 2 generated by the unstabilized (left) and stabilized (right) Lagrange multipliers method.

We then write the variation $\boldsymbol{\eta}$ in a form similar to the trial function $\boldsymbol{u}$ (see Eq. (2))

$$\boldsymbol{\eta} = \bar{\boldsymbol{\eta}} + M_{\mathcal{S}}\tilde{\boldsymbol{\eta}}, \tag{14}$$

where $\bar{\boldsymbol{\eta}}$ and $M_{\mathcal{S}}\tilde{\boldsymbol{\eta}}$ are the continuous and discontinuous parts of $\boldsymbol{\eta}$, respectively. Without loss of generality, we assume that the support Ω^h has a null intersection with Dirichlet boundary Γ_{g_i}. Thus, $\bar{u}_i \in \mathcal{U}_i$ and $\bar{\eta}_i \in \mathcal{V}_i$, whereas $(\tilde{u}_i, \tilde{\eta}_i) \in \mathcal{H}$, where $\mathcal{H}$ is simply the collection of H^1 functions.

The variational equation takes the form

$$\int_{\Omega\setminus\mathcal{S}} \nabla^s \boldsymbol{\eta} : \boldsymbol{\sigma} d\Omega + \int_{\Omega\setminus\mathcal{S}} \boldsymbol{\eta}\cdot\boldsymbol{f} d\Omega + \int_{\Gamma_h} \boldsymbol{\eta}\cdot\boldsymbol{h} d\Gamma + \mathcal{G}_c = 0, \tag{15}$$

where

$$\mathcal{G}_c = \int_{\tilde{\mathcal{S}}_-} \boldsymbol{\eta}_-\cdot\boldsymbol{t}_- d\mathcal{S}_- + \int_{\tilde{\mathcal{S}}_+} \boldsymbol{\eta}_+\cdot\boldsymbol{t}_+ d\mathcal{S}_+ = -\int_{\tilde{\mathcal{S}}} \tilde{\boldsymbol{\eta}}\cdot\boldsymbol{t} d\mathcal{S}, \tag{16}$$

and $\boldsymbol{t}=\boldsymbol{t}_-$ is the traction vector acting on the negative face of the crack. Using decomposition (Eq. (14)), and noting that $\bar{\boldsymbol{\eta}}$ and $\tilde{\boldsymbol{\eta}}$ are two independent variations, we obtain the pair of variational equations

$$\int_{\Omega\setminus\mathcal{S}} \nabla^s \bar{\boldsymbol{\eta}} : \boldsymbol{\sigma} d\Omega + \int_{\Omega\setminus\mathcal{S}} \bar{\boldsymbol{\eta}}\cdot\boldsymbol{f} d\Omega + \int_{\Gamma_h} \bar{\boldsymbol{\eta}}\cdot\boldsymbol{h} d\Gamma = 0, \tag{17}$$

and

$$\int_{\Omega\setminus\mathcal{S}} \nabla^s (M_{\mathcal{S}}\tilde{\boldsymbol{\eta}}) : \boldsymbol{\sigma} d\Omega + \int_{\Omega\setminus\mathcal{S}} (M_{\mathcal{S}}\tilde{\boldsymbol{\eta}})\cdot\boldsymbol{f} d\Omega + \int_{\Gamma_h} (M_{\mathcal{S}}\tilde{\boldsymbol{\eta}})\cdot\boldsymbol{h} d\Gamma + \mathcal{G}_c = 0. \tag{18}$$

The Lagrange multipliers method entails treating the normal component of traction, which takes the role of the Lagrange multiplier, as an independent variable. We denote this normal traction on $\mathcal{S}$ by $\lambda \geq 0$ and its associated variation by $\psi \geq 0$. In general there are no boundary conditions for the functions λ and ψ, and here we require that they simply satisfy the set relation $(\lambda,\psi) \in \mathcal{P}$, where $\mathcal{P}$ is a collection of nonnegative L_2 functions. The complete traction vector is given by

$$\boldsymbol{t} = \boldsymbol{t}_T - \lambda\boldsymbol{n}. \tag{19}$$

If the active contact surface $\tilde{\mathcal{S}} \subset \mathcal{S}$ is known, so that $\lambda,\psi>0$ on $\tilde{\mathcal{S}}$ and $\lambda=\psi=0$ on $\mathcal{S}\setminus\tilde{\mathcal{S}}$ (opening mode), then the surface integral $\mathcal{G}_c$ reduces to the form

$$\mathcal{G}_c = -\int_{\tilde{\mathcal{S}}} \tilde{\boldsymbol{\eta}}\cdot\boldsymbol{t}_T d\mathcal{S} + \int_{\tilde{\mathcal{S}}} \lambda(\tilde{\boldsymbol{\eta}}\cdot\boldsymbol{n}) d\mathcal{S}. \tag{20}$$

In this case the KKT conditions collapse to the simpler form

$$\lambda(\boldsymbol{x}) > 0, \qquad h(\boldsymbol{x}) = 0, \qquad \forall \boldsymbol{x} \in \tilde{\mathcal{S}}. \tag{21}$$

The above constraints can be converted into a weighted integral of the form

$$\int_{\tilde{\mathcal{S}}} \psi(\boldsymbol{x})\tilde{\boldsymbol{u}}(\boldsymbol{x})\cdot\boldsymbol{n}(\boldsymbol{x}) d\mathcal{S} = 0. \tag{22}$$

Eqs. (17), (18), and (22) constitute a three-field $\{\bar{\boldsymbol{u}}, \tilde{\boldsymbol{u}}, \lambda\}$ mixed variational formulation.

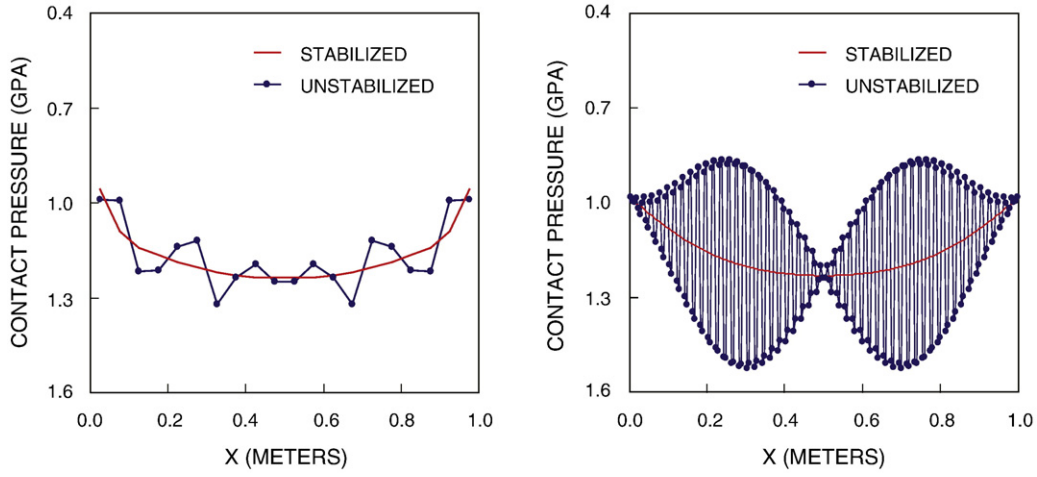

Fig. 6. Stabilized and unstabilized contact pressures calculated by Lagrange multipliers method: Mesh 1 (left) and Mesh 2 (right). All contact segments are of equal length.

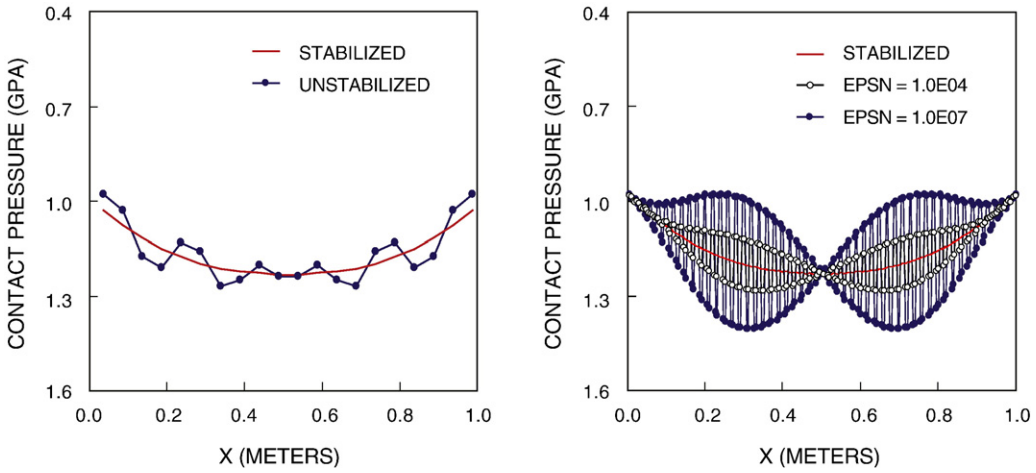

Fig. 7. Stabilized and unstabilized contact pressures calculated by penalty method: Mesh 1 with $\epsilon_N = 10^7$ GPa/m (left) and Mesh 2 with $\epsilon_N = 10^4$ and 10^7 GPa/m (right). All contact segments are of equal length. Note that contact pressure oscillation from the unstabilized solution is weaker with a lower penalty parameter, but interpenetration of the contact faces is greater. However, the stabilized solution suppresses any such oscillation irrespective of the value of the penalty parameter.

The penalty formulation entails expressing the Lagrange multiplier $\lambda(\boldsymbol{x})$ in terms of the gap function $h(\boldsymbol{x})$ via a constitutive equation of the form

$$\lambda(\boldsymbol{x}) = \epsilon_N h(\boldsymbol{x}) \geq 0, \qquad \forall \boldsymbol{x} \in \tilde{\mathcal{S}}, \tag{23}$$

where $\epsilon_N \gg 1$ is a penalty parameter. The normal contact pressure λ becomes H^1 since $h(\boldsymbol{x})$ is an H^1 function. The traction vector $\boldsymbol{t}$ in Eq. (19) becomes

$$\boldsymbol{t} = \boldsymbol{t}_T - \epsilon_N (\tilde{\boldsymbol{u}} \cdot \boldsymbol{n}) \boldsymbol{n}. \tag{24}$$

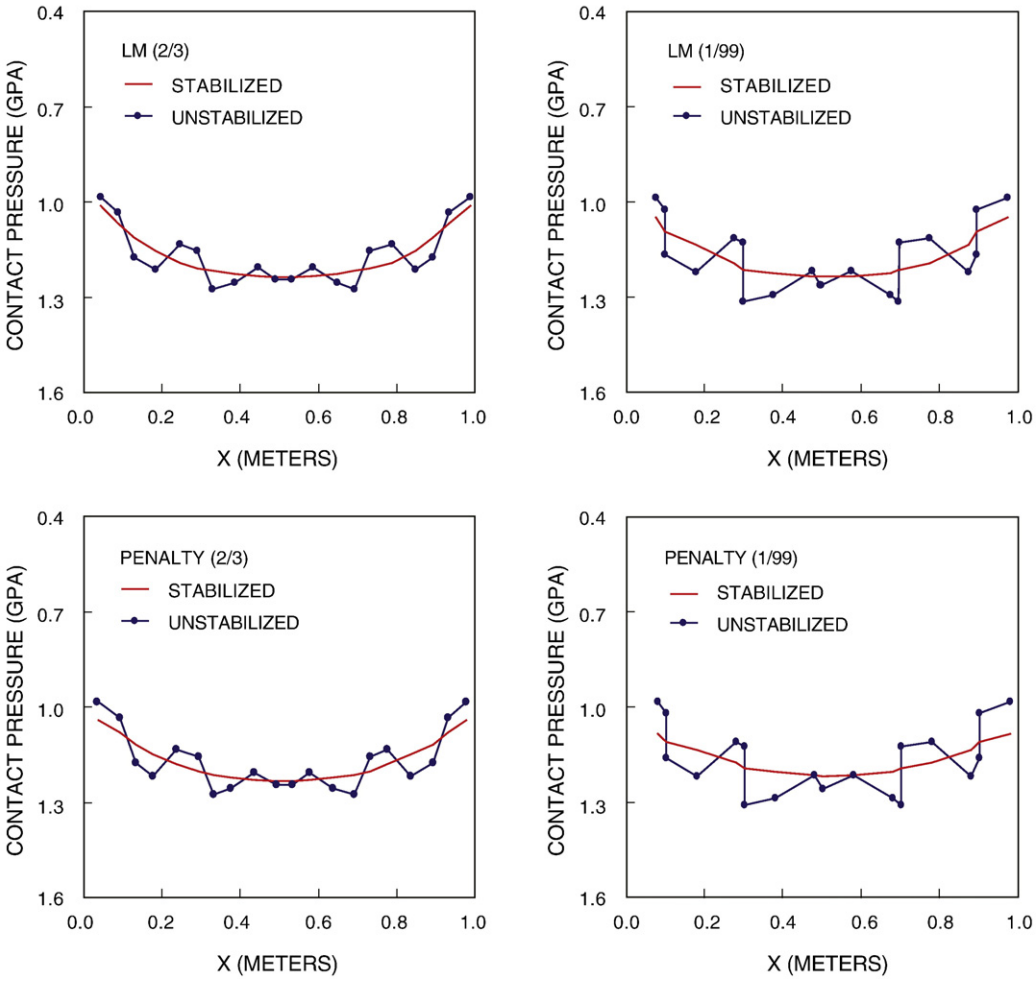

Fig. 8. Stabilized and unstabilized contact pressures calculated by Lagrange multipliers and penalty methods with Mesh 1. Numbers in parentheses are segment length ratios.

The idea behind the penalty formulation is to prescribe a very large value of penalty parameter ϵ_N to force h to become small, thus approximately satisfying the interpenetration condition (22).

3. Stabilized finite element formulation

We introduce approximations to trial functions, $\{\tilde{\boldsymbol{u}}^h, \tilde{\boldsymbol{u}}^h, \lambda^h\}$, and their associated variations, $\{\bar{\boldsymbol{\eta}}^h, \tilde{\boldsymbol{\eta}}^h, \psi^h\}$, where $\tilde{u}_i^h + M_S\tilde{u}_i^h \in \mathcal{U}_i^h$, $\bar{\eta}_i^h + M_S\tilde{\eta}_i^h \in \mathcal{V}_i^h$, and $(\lambda^h, \psi^h) \in \mathcal{P}^h$. Here, $\mathcal{U}_i^h \subset \mathcal{U}_i$, $\mathcal{V}_i^h \subset \mathcal{V}_i$, and $\mathcal{P}^h \subset \mathcal{P}$ are the corresponding finite dimensional trial/weighting subspaces. Substituting in the variational equations yields

$$\int_{\Omega\setminus\mathcal{S}} \nabla^s \bar{\boldsymbol{\eta}}^h : \boldsymbol{\sigma}(\boldsymbol{u}^h)d\Omega + \int_{\Omega\setminus\mathcal{S}} \bar{\boldsymbol{\eta}}^h \cdot \boldsymbol{f} d\Omega + \int_{\Gamma_h} \bar{\boldsymbol{\eta}}^h \cdot \boldsymbol{h} d\Gamma = 0, \tag{25}$$

$$\int_{\Omega\setminus\mathcal{S}} \nabla^s \left(M_S\tilde{\boldsymbol{\eta}}^h\right) : \boldsymbol{\sigma}(\boldsymbol{u}^h)d\Omega + \int_{\Omega\setminus\mathcal{S}} \left(M_S\tilde{\boldsymbol{\eta}}^h\right) \cdot \boldsymbol{f} d\Omega + \int_{\Gamma_h} \left(M_S\tilde{\boldsymbol{\eta}}^h\right) \cdot \boldsymbol{h} d\Gamma - \int_{\tilde{\mathcal{S}}} \tilde{\boldsymbol{\eta}}^h \cdot \boldsymbol{t}_T d\mathcal{S} + \int_{\tilde{\mathcal{S}}} \left(\tilde{\boldsymbol{\eta}}^h \cdot \boldsymbol{n}\right) \lambda^h d\mathcal{S} = 0, \tag{26}$$

and

$$\int_{\tilde{\mathcal{S}}} \psi^h \tilde{\boldsymbol{u}}^h \cdot \boldsymbol{n} d\mathcal{S} = 0. \tag{27}$$

The above equations have striking semblance with the mixed formulation for Stokes equation, which is known to produce numerical instabilities for certain combinations of velocity and pressure approximations. For Stokes equation it is known that the discrete velocity and pressure spaces, $\boldsymbol{\mathcal{U}}^h$ and $\mathcal{P}^h$, respectively, must be chosen to satisfy the discrete LBB condition

$$\sup_{\boldsymbol{v}^h \in \boldsymbol{\mathcal{U}}^h} \frac{\int_\Omega \psi^h \nabla \cdot \boldsymbol{v}^h d\Omega}{\|\boldsymbol{v}^h\|_1} \geq c\|\psi^h\|_0 \qquad \forall \psi^h \in \mathcal{P}^h, \tag{28}$$

with $C>0$ independent of h. Unfortunately, many linear-pressure/linear-velocity interpolations do not satisfy this condition and lead to unstable approximations. However, Bochev and co-workers [6,7] demonstrated that this linear pair does satisfy the weaker condition,

$$\sup_{\boldsymbol{v}^h \in \boldsymbol{\mathcal{U}}^h} \frac{\int_\Omega \psi^h \nabla \cdot \boldsymbol{v}^h d\Omega}{\|\boldsymbol{v}^h\|_1} \geq C_1\|\psi^h\|_0 - C_2\|\psi^h - \Pi\psi^h\|_0 \qquad \forall \psi^h \in \mathcal{P}^h, \tag{29}$$

where Π: $L_2(\Omega) \to R_0$ is a projection operator and R_0 is the space of piecewise constants, and with $C_1>0$ and $C_2>0$ independent of h. The term $C_2\|q^h - \Pi q^h\|_0$ quantifies the inherent deficiency in the linear pair and motivates a similar stabilization approach for the contact problem.

The stabilization methodology advocated in this paper is to add stabilizing terms to the variational Eq. (27) to penalize the deficiency in the displacement and contact pressure approximations. The stabilized variational equation takes the form

$$\int_{\tilde{\mathcal{S}}} \psi^h \tilde{\boldsymbol{u}}^h \cdot \boldsymbol{n}^h d\mathcal{S} - \int_{\tilde{\mathcal{S}}} \frac{\tau}{2M} \left(\psi^h - \Pi\psi^h\right)\left(\lambda^h - \Pi\lambda^h\right) d\mathcal{S} = 0, \tag{30}$$

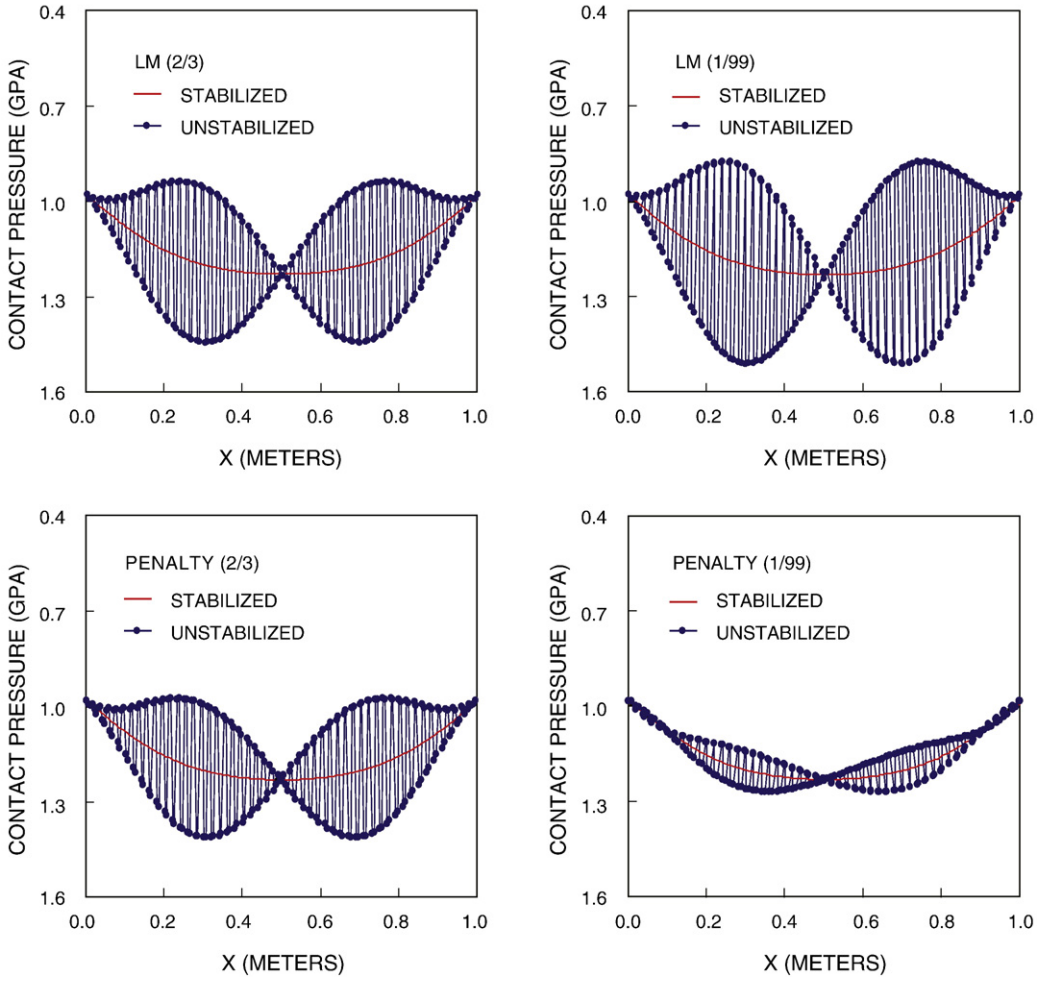

Fig. 9. Stabilized and unstabilized contact pressures calculated by Lagrange multipliers and penalty methods with Mesh 2. Numbers in parentheses are segment length ratios.

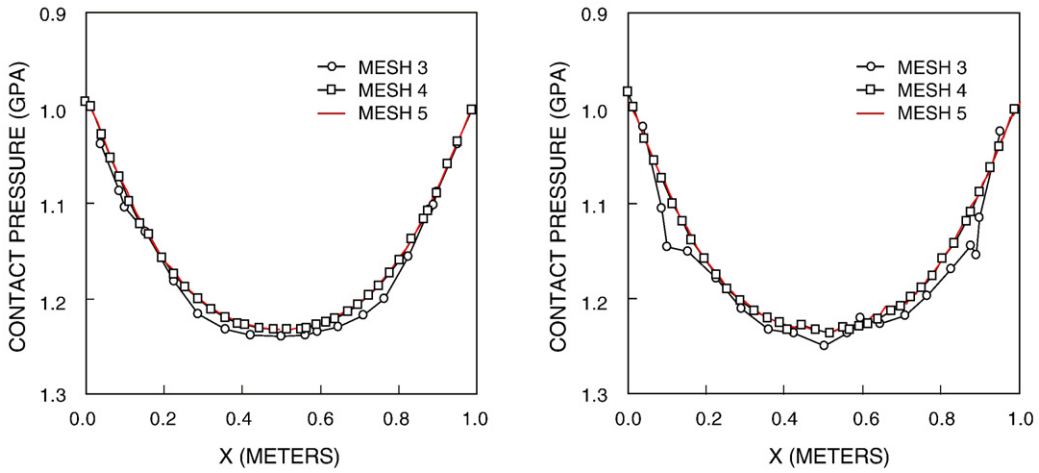

Fig. 10. Mesh convergence study: stabilized contact pressures calculated by Lagrange multipliers method (left) and penalty method (right).

where M is a volume modulus of the bulk material (similar in meaning to the Winkler modulus in beam-on-elastic-foundation theory), and $\tau>0$ is a constant multiplier, or stabilization parameter. The parameter M has the physical meaning of being the pressure necessary to produce a unit indentation in the bulk material, and for the present case this parameter may be taken to be numerically equal to the Young's modulus of elasticity of the bulk material but with units of F/L^3. The dimensionless parameter τ, on the other hand, serves to "tune" the stabilization and has been normalized in the above equation to have a value on the order 1.0. For linear displacement interpolation the projection operator Π may be evaluated from the volume mean

$$\Pi\lambda^h|_{\Omega^e} = \frac{1}{V^e}\int_{\Omega^e}\lambda^h d\Omega^e. \tag{31}$$

For 2D problems the above definition reduces to an area mean.

To demonstrate the implications of the stabilizing terms on the FE matrix equations, consider a linear elastic bulk material with frictionless contact and assume linear triangular finite elements for the compact support Ω^h. Interpolation of the trial functions inside an enriched element Ω^e yields

$$\bar{u}_i^h = \sum_{A=1}^{3} N_A d_{iA}^e, \qquad \tilde{u}_i^h = \sum_{A=1}^{3} N_A a_{iA}^e, \qquad \lambda^h = \sum_{A=1}^{3} N_A \lambda_A^e, \tag{32}$$

where d_{iA}^e, a_{iA}^e, and λ_A^e are, respectively, the regular displacement, slip, and normal contact pressure nodal degrees of freedom in the enriched element. In matrix form, we write

$$\bar{\boldsymbol{u}}^h = \boldsymbol{N}\boldsymbol{d}, \qquad \tilde{\boldsymbol{u}}^h = \boldsymbol{N}\boldsymbol{a}, \qquad \lambda^h = \bar{\boldsymbol{N}}\boldsymbol{\lambda}, \tag{33}$$

where $\overline{\boldsymbol{N}}$ is the compact version of $\boldsymbol{N}$ appropriate for interpolating a scalar field. Thus, the nodes of an enriched finite element Ω^e now also contain slip and contact pressure degrees of freedom, in addition to the standard displacement degrees of freedom (for a total of five degrees of freedom in 2D). An enriched CST element is shown in Fig. 2.

The system of equations to solve in a Lagrange multipliers formulation with frictionless contact has a block-partitioned structure of the form

$$\begin{bmatrix} \boldsymbol{K}_{11} & \boldsymbol{K}_{12} & \boldsymbol{0} \\ \boldsymbol{K}_{21} & \boldsymbol{K}_{22} & \boldsymbol{K}_{23} \\ \boldsymbol{0} & \boldsymbol{K}_{32} & \boldsymbol{K}_{33} \end{bmatrix} \begin{Bmatrix} \boldsymbol{d} \\ \boldsymbol{a} \\ \boldsymbol{\lambda} \end{Bmatrix} = \begin{Bmatrix} \boldsymbol{F}_1 \\ \boldsymbol{F}_2 \\ \boldsymbol{0} \end{Bmatrix}, \tag{34}$$

where the submatrices are given by (see [8,28] for details)

$$\begin{aligned} \boldsymbol{K}_{11} &= \int_\Omega \boldsymbol{B}^T\boldsymbol{D}\boldsymbol{B}d\Omega, & \boldsymbol{K}_{12} &= \int_\Omega \boldsymbol{B}^T\boldsymbol{D}\tilde{\boldsymbol{B}}d\Omega = \boldsymbol{K}_{21}^T, \\ \boldsymbol{K}_{22} &= \int_\Omega \tilde{\boldsymbol{B}}^T\boldsymbol{D}\tilde{\boldsymbol{B}}d\Omega, & \boldsymbol{K}_{23} &= \int_{\tilde{S}} (\boldsymbol{n}\boldsymbol{N})^T\bar{\boldsymbol{N}}d\mathcal{S} = \boldsymbol{K}_{32}^T, \\ \boldsymbol{K}_{33} &= -\int_{\tilde{S}} \frac{\tau}{2M}\left(\bar{\boldsymbol{N}} - \Pi\,\bar{\boldsymbol{N}}\right)^T\left(\bar{\boldsymbol{N}} - \Pi\,\bar{\boldsymbol{N}}\right)d\mathcal{S}, \end{aligned} \tag{35}$$

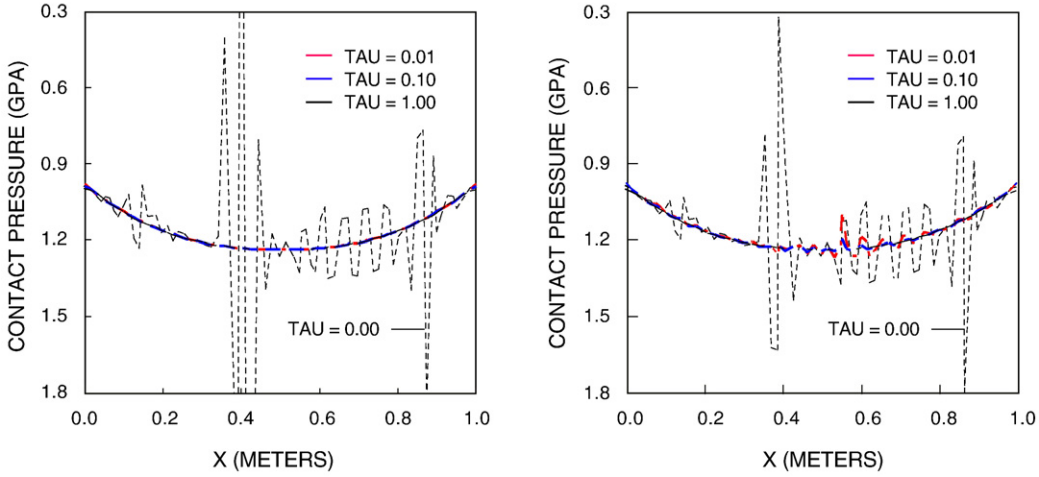

Fig. 11. Influence of stabilization parameter τ on contact pressure distribution using Mesh 4: Lagrange multipliers method (left) and penalty method (right). Unstabilized formulation has $\tau=0.00$.

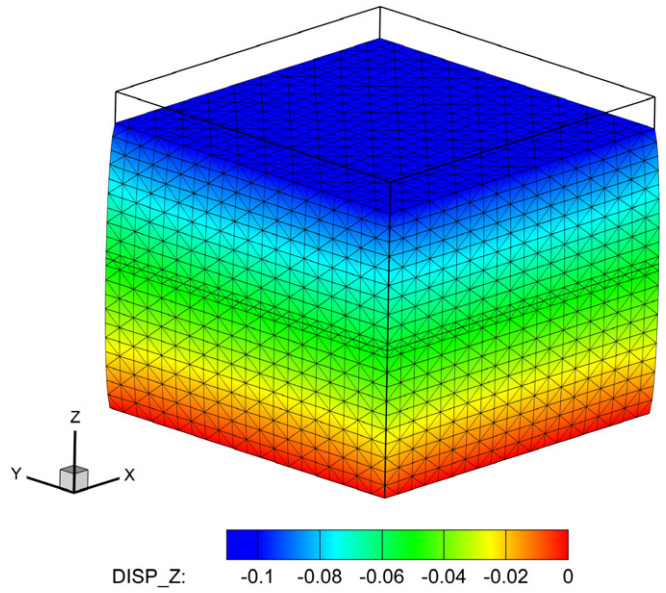

Fig. 12. Deformed finite element mesh for 3D elastic blocks with frictionless contact under vertical compression.

and where $\boldsymbol{D}$ is the constitutive stress–strain matrix, and $\boldsymbol{B}$ and $\tilde{\boldsymbol{B}}$ are the strain–displacement transformation matrices. We should note that for a CST element the projection operator Π operates on the shape function matrix $\boldsymbol{N}$ as follows

$$\Pi N_A = \frac{1}{3}, \qquad A = 1,2,3. \tag{36}$$

Similarly, for a 3D tetrahedral element the projection operator Π operates on the shape function matrix $\boldsymbol{N}$ according to the rule

$$\Pi N_A = \frac{1}{4}, \qquad A = 1,2,3,4. \tag{37}$$

If the contact surface $\tilde{\mathcal{S}}$ is to be determined iteratively, and/or if the bulk material undergoes plastic deformation, then the above matrix equation may be viewed as the relevant tangent operator in the linearized system. Note that without a stabilizing term a null submatrix $\boldsymbol{K}_{33} = \boldsymbol{0}$ appears in the (3,3) block of Eq. (34).

As noted in the beginning, the Lagrange multipliers formulation has a drawback in that it is very difficult to implement the technique when the problem involves frictional contact. A far simpler formulation is provided by the penalty method, although this, too, suffers from numerical instabilities unless the formulation is stabilized. Fortunately, the penalty method is also amenable to PPP stabilization. Eqs. (25) and (26) constitute the relevant equations in the penalty formulation, but here we stabilize the latter equation by adding once again the stabilization term.

We first consider the slip case where the tangential traction is calculated based on the normal contact pressure through the coefficient of friction. By stabilizing the normal contact pressure we stabilize the tangential component as well. Hence, it suffices to write

$$\int_{\Omega\setminus\mathcal{S}} \nabla^s\left(M_{\mathcal{S}}\tilde{\boldsymbol{\eta}}^h\right) : \boldsymbol{\sigma}(\boldsymbol{u}^h)d\Omega + \int_{\Omega\setminus\mathcal{S}}\left(M_{\mathcal{S}}\tilde{\boldsymbol{\eta}}^h\right)\cdot\boldsymbol{f}\,d\Omega + \int_{\Gamma_h}\left(M_{\mathcal{S}}\tilde{\boldsymbol{\eta}}^h\right)\cdot\boldsymbol{h}d\Gamma$$
$$-\int_{\tilde{\mathcal{S}}}\tilde{\boldsymbol{\eta}}^h\cdot\boldsymbol{t}d\mathcal{S} - \int_{\tilde{\mathcal{S}}}\frac{\tau}{2M}(\psi^h - \Pi\psi^h)(\lambda^h - \Pi\lambda^h)d\mathcal{S} = 0. \tag{38}$$

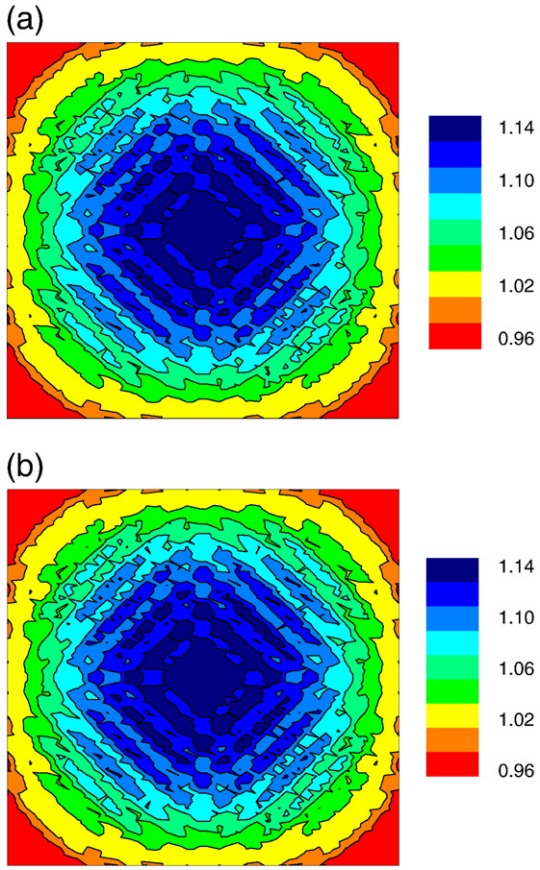

Fig. 13. Unstabilized normal contact pressure (in GPa) on frictionless contact face: (a) Lagrange multipliers; (b) penalty method with $\epsilon_N = 10^7$ GPa/m.

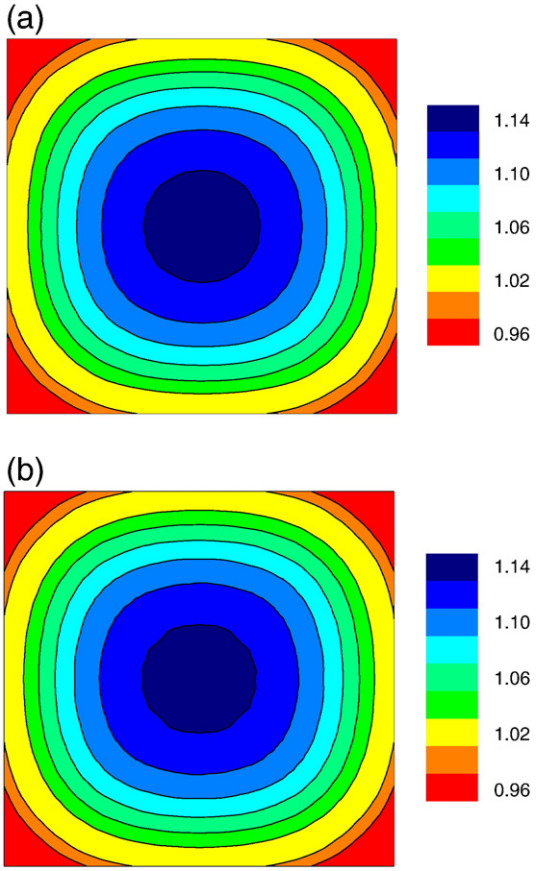

Fig. 14. Stabilized normal contact pressure (in GPa) on frictionless contact face: (a) Lagrange multipliers; (b) penalty method with $\epsilon_N = 10^7$ GPa/m.

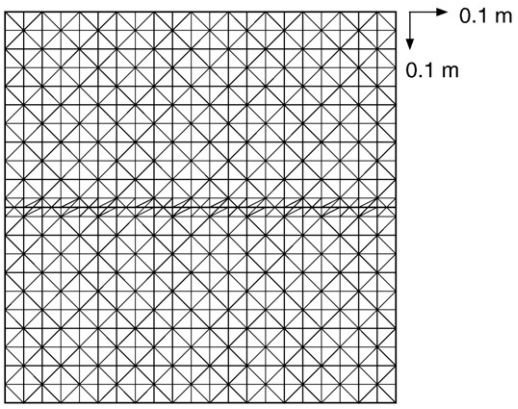

Fig. 15. FE mesh for plane strain compression and shearing of elastic plate with a horizontal glued crack: the mesh has 484 nodes and 882 CST elements.

Observe that we have written the full traction vector $\boldsymbol{t}$ in the crack surface integral, implying that we are now in a position to handle frictional sliding as well.

Using Eq. (23) we express the trial functions and variations for the normal contact pressures in terms of the gap functions as

$$\lambda^h|_{\mathcal{S}} = \epsilon_N \tilde{\boldsymbol{u}}^h \cdot \boldsymbol{n}|_{\mathcal{S}}, \qquad \psi^h|_{\mathcal{S}} = \epsilon_N \tilde{\boldsymbol{\eta}}^h \cdot \boldsymbol{n}|_{\mathcal{S}}. \tag{39}$$

Thus, Eq. (38) becomes

$$\int_{\Omega\setminus\mathcal{S}} \boldsymbol{\nabla}^s\left(M_{\mathcal{S}}\tilde{\boldsymbol{\eta}}^h\right) : \boldsymbol{\sigma}(\boldsymbol{u}^h)d\Omega + \int_{\Omega\setminus\mathcal{S}}\left(M_{\mathcal{S}}\tilde{\boldsymbol{\eta}}^h\right)\cdot\boldsymbol{f}d\Omega + \int_{\Gamma_h}\left(M_{\mathcal{S}}\tilde{\boldsymbol{\eta}}^h\right)\cdot\boldsymbol{h}d\Gamma$$
$$-\int_{\tilde{\mathcal{S}}}\tilde{\boldsymbol{\eta}}^h\cdot\boldsymbol{t}d\mathcal{S} - \int_{\tilde{\mathcal{S}}}\frac{\tau\epsilon_N^2}{2M}\left(\tilde{\boldsymbol{\eta}}^h - \Pi\tilde{\boldsymbol{\eta}}^h\right)\cdot(\boldsymbol{n}\otimes\boldsymbol{n})\cdot\left(\tilde{\boldsymbol{u}}^h - \Pi\tilde{\boldsymbol{u}}^h\right)d\mathcal{S} = 0. \tag{40}$$

The formulation thus reduces to that presented in [8,28] except with the additional stabilizing term. The final block-partitioned matrix equation has the form

$$\begin{bmatrix}\boldsymbol{K}_{11} & \boldsymbol{K}_{12}\\ \boldsymbol{K}_{21} & (\boldsymbol{K}_{22}+\boldsymbol{K}_{\text{stab}})\end{bmatrix}\begin{Bmatrix}\boldsymbol{d}\\ \boldsymbol{a}\end{Bmatrix} = \begin{Bmatrix}\boldsymbol{F}_1\\ \boldsymbol{F}_2\end{Bmatrix}, \tag{41}$$

where

$$\boldsymbol{K}_{\text{stab}} = \int_{\tilde{\mathcal{S}}}\frac{\tau}{2M}(\boldsymbol{N}-\Pi\boldsymbol{N})^T\boldsymbol{E}(N-\Pi\boldsymbol{N})d\mathcal{S} \tag{42}$$

and

$$\boldsymbol{E} = \epsilon_N^2\boldsymbol{n}\boldsymbol{n}^T. \tag{43}$$

Next we consider the stick case where the normal and tangential components of traction are calculated independently, and therefore

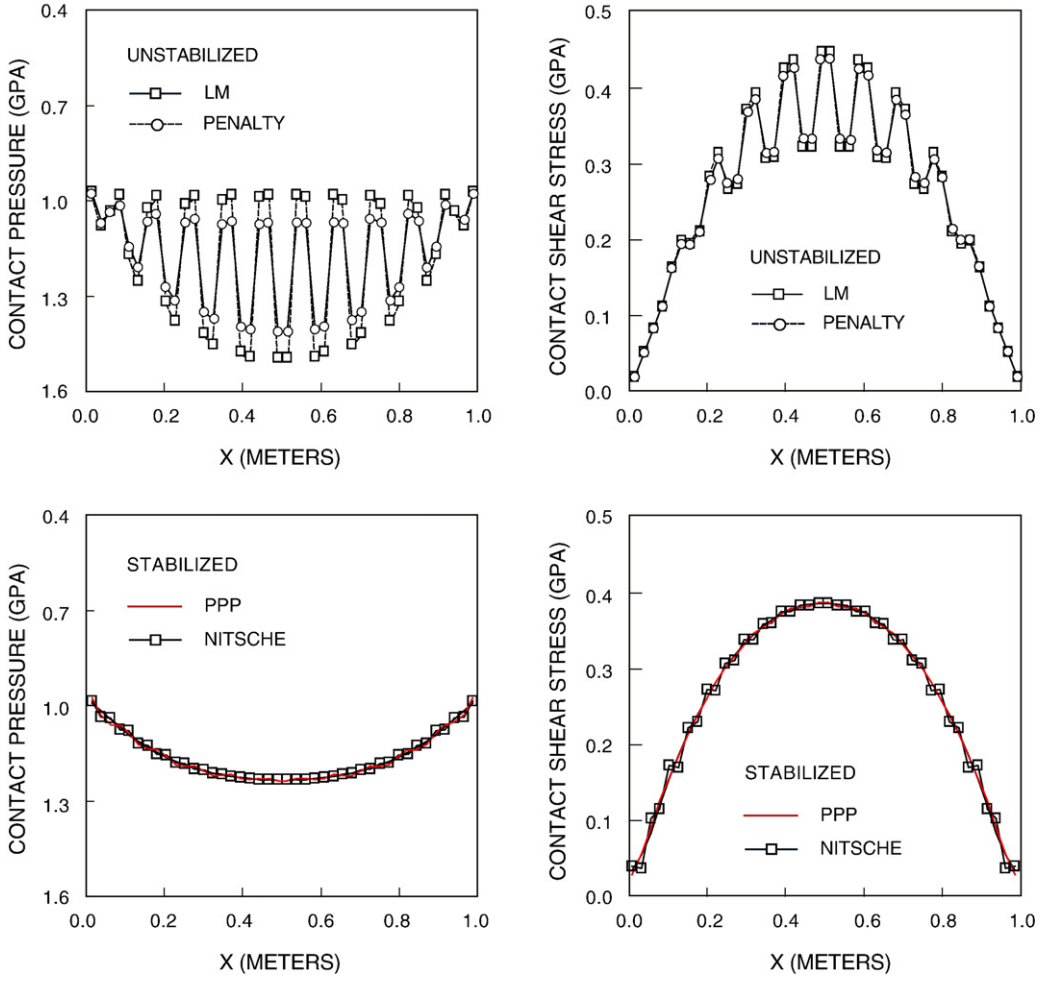

Fig. 16. Unstabilized and stabilized contact pressures and shear stresses calculated by Lagrange multipliers and penalty methods with Mesh 2. The lower two figures compare the stabilized solutions obtained by the PPP and Nitsche's stabilization techniques.

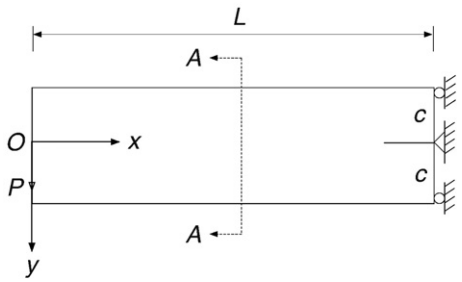

Fig. 17. Spatial convergence study: plane stress bending of a beam.

must be stabilized separately. The stabilized variational equation is now written as

$$\int_{\Omega\setminus\mathcal{S}} \nabla^s\left(M_{\mathcal{S}}\tilde{\boldsymbol{\eta}}^h\right) : \boldsymbol{\sigma}(\boldsymbol{u}^h)d\Omega + \int_{\Omega\setminus\mathcal{S}}\left(M_{\mathcal{S}}\tilde{\boldsymbol{\eta}}^h\right)\cdot\boldsymbol{f}d\Omega + \int_{\Gamma_h}\left(M_{\mathcal{S}}\tilde{\boldsymbol{\eta}}^h\right)\cdot\boldsymbol{h}d\Gamma$$
$$-\int_{\tilde{\mathcal{S}}}\tilde{\boldsymbol{\eta}}^h\cdot\boldsymbol{t}d\mathcal{S}-\int_{\tilde{\mathcal{S}}}\frac{\tau}{2M}\left(\psi^h-\Pi\psi^h\right)\left(\lambda^h-\Pi\lambda^h\right)d\mathcal{S}$$
$$-\int_{\tilde{\mathcal{S}}}\frac{\tau}{2M}\left(\psi_T^h-\Pi\psi_T^h\right)\left(\lambda_T^h-\Pi\lambda_T^h\right)d\mathcal{S}=0, \tag{44}$$

where λ_T^h is the tangential component of traction with associated variation ψ_T^h. A stick condition is obtained by penalization of the tangential terms in the form

$$\lambda_T^h|_{\mathcal{S}} = \epsilon_T\tilde{\boldsymbol{u}}^h\cdot\boldsymbol{\mu}|_{\mathcal{S}}, \qquad \psi_T^h|_{\mathcal{S}} = \epsilon_T\tilde{\boldsymbol{\eta}}^h\cdot\boldsymbol{\mu}|_{\mathcal{S}}, \tag{45}$$

in which $\epsilon_T \gg 1$ is the tangential penalty parameter and $\boldsymbol{\mu}$ is the unit tangent vector (i.e., $\boldsymbol{\mu}\cdot\boldsymbol{n}=0$). An additional stabilization term can be inserted simply by using the same expression for $\boldsymbol{K}_{\text{stab}}$ in Eq. (42) but with

$$\boldsymbol{E} = \epsilon_N^2\boldsymbol{n}\boldsymbol{n}^T + \epsilon_T^2\boldsymbol{\mu}\boldsymbol{\mu}^T. \tag{46}$$

4. Numerical examples

This section presents the results of numerical simulations on a variety of 2D plane strain, plane stress, and 3D problems using enriched constant strain triangular (CST) elements (for 2D) and enriched constant strain tetrahedral elements (for 3D). The first set of simulations deals with frictionless contact and demonstrates the performance of the stabilized Lagrange multipliers and penalty techniques. The second set deals with frictional contact and assesses the performance of the stabilized penalty formulation.

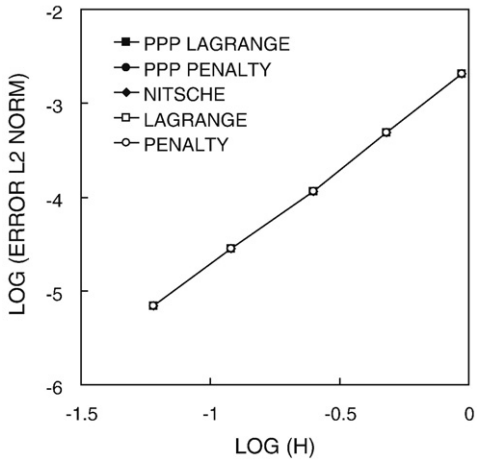

Fig. 18. Spatial convergence profiles in L^2-norm of error in displacement field for the beam bending problem. "Lagrange" and "penalty" are the unstabilized solutions.

4.1. Plane strain frictionless contact

The problem of interest is a 1.0 m by 1.0 m (square) elastic plate with a horizontal smooth crack passing through the middle of the plate. The bulk material has a Young's modulus of elasticity $E=10$ GPa and Poisson's ratio $\nu=0.30$. The plate is clamped at both its top and bottom boundaries. A vertical downward displacement of -0.10 m is then prescribed at the top boundary while holding the bottom boundary fixed. This causes the crack faces to press against each other as the plate is compressed vertically. Unless otherwise noted, the stabilization parameter is set to $\tau=1.0$ and the penalty parameter is $\epsilon_N=10^7$ GPa/m in all the simulations.

For the numerical simulations we consider five FE meshes: two structured (Meshes 1 and 2 in Fig. 3) and three unstructured (Meshes 3, 4 and 5 in Fig. 4). The structured meshes have the CSTs oriented upright in cross-diagonal pattern to minimize element bias, whereas the unstructured meshes have the CSTs oriented in arbitrary directions. Before proceeding with a comparison of the stabilized and unstabilized contact pressures, we show in Fig. 5 the nearly identical contours of horizontal displacements generated using Mesh 2 with and without stabilization. These results are typical and show that in general the numerical instability does not afflict the overall displacement pattern, but rather, it mainly gives rise to the undesirable contact pressure oscillation.

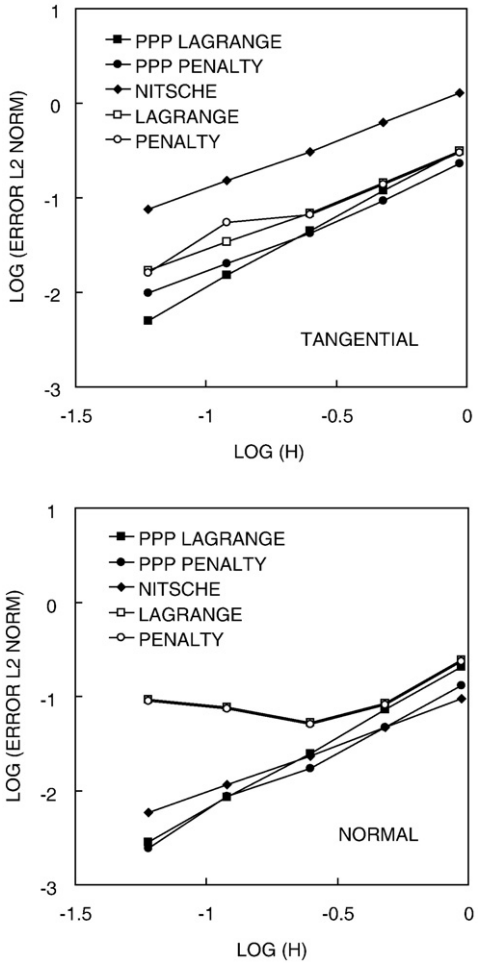

Fig. 19. Spatial convergence profiles in L^2-norm of errors in the traction field on section A–A: tangential traction (top), and normal traction (bottom). "Lagrange" and "penalty" are the unstabilized solutions. The PPP-stabilized Lagrange multipliers method has the fastest convergence rate (steepest slope) in both the normal and tangential components of traction, whereas the Nitsche-stabilized solution has the largest error in the tangential traction for a given mesh.

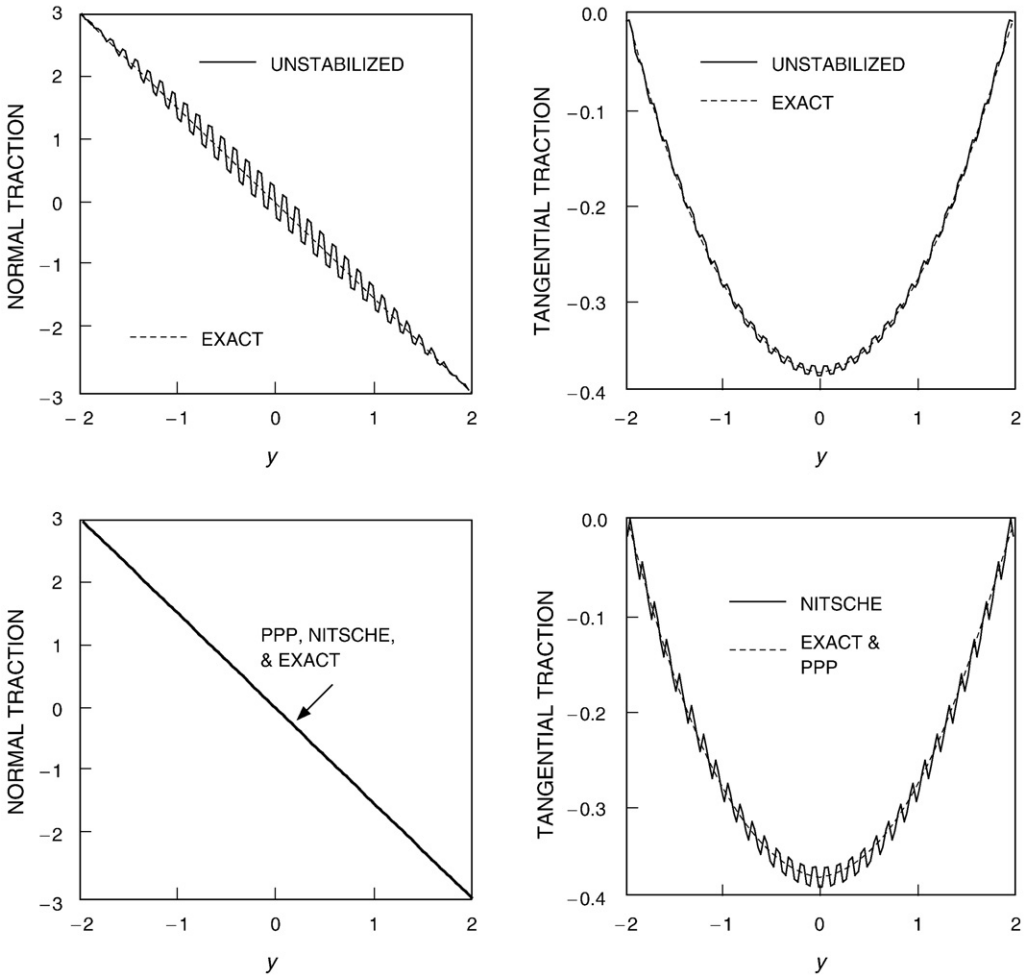

Fig. 20. Unstabilized and stabilized contact pressures and shear stresses on section *A–A* for the elastic beam plane stress problem using a structured mesh with 16,770 nodes and 32,896 CST elements. The lower two figures compare the PPP- and Nitsche-stabilized solutions with the exact solution. Note that for this mesh the PPP-stabilized solutions are nearly the same as the exact solution in both the normal and tangential components of traction. On the other hand, Nitsche's method stabilized the normal component of traction but oscillations in the tangential traction got worse compared to the unstabilized solution.

By adjusting the vertical position of the horizontal crack, we generate the configurations shown in Fig. 3 in which the crack faces are defined by line segments of equal length. Figs. 6 and 7 show the contact pressure distributions calculated by the Lagrange multipliers and penalty methods. Note that oscillation in contact pressures deteriorates as the mesh is refined, clearly suggesting that this feature is a numerical instability and not a physical response. Furthermore, oscillation is stronger in the Lagrange multipliers solutions, where contact condition is enforced exactly, than in the penalty solutions, where contact condition is enforced only approximately. In contrast, no oscillation whatsoever can be detected from the stabilized Lagrange multipliers and penalty solutions. The calculated values of contact pressure from the stabilized solutions, on the order 1.0–1.3 GPa, check with the lower limit of 1 GPa if the top and bottom boundaries of the plate were free to move horizontally, and with the upper limit of 1.35 GPa if the two vertical boundaries were prevented from displacing horizontally.

To investigate how the uneven discretization of the crack geometry influences the contact pressure oscillation, we move the crack slightly in the vertical direction so that it is now defined by alternating short-long segments derived from the enriched CST elements. Two positions are considered, defined by segment length ratios of 2/3 and 1/99. In the latter segment length ratio, the crack is nearly coincident with a horizontal row of nodes so that it nearly cuts through the corners and bases of adjacent triangles in alternating fashion. Figs. 8 and 9 show the distributions of contact pressure generated by the stabilized and unstabilized solutions using Meshes 1 and 2, respectively. Once again, the unstabilized Lagrange multipliers solutions show a propensity to oscillate more violently compared with the unstabilized penalty solutions. Furthermore, with Mesh 1 the pressure oscillation resulting from the unstabilized solutions seems to deteriorate as the segment length ratio increases, but with Mesh 2 an opposite trend is observed from the unstabilized penalty solutions. These trends, or lack thereof,

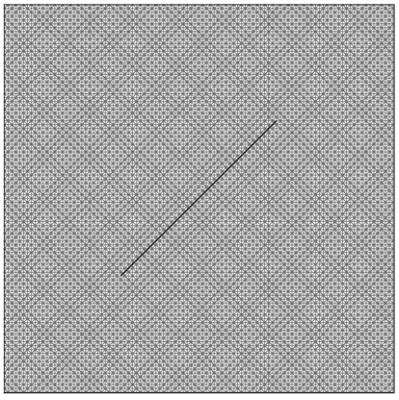

Fig. 21. FE mesh for elasto-plastic plate with a diagonal crack: the mesh has 10,000 nodes and 20,000 CST elements, and deforming in plane strain.

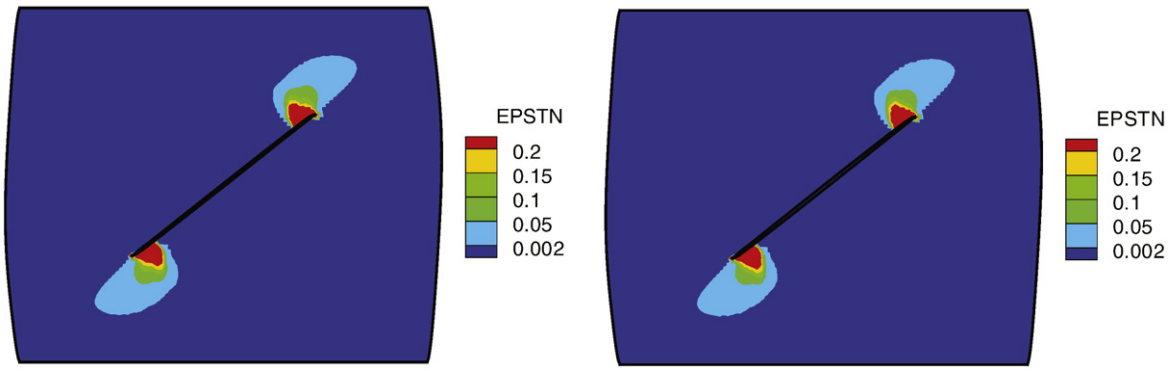

Fig. 22. Contours of plastic strain after a nominal vertical compression of 10% from stabilized (left) and unstabilized (right) solutions.

are immaterial in light of the effectiveness of the proposed stabilization technique, which completely eliminates any oscillation with both the Lagrange multipliers and penalty solutions. We should note that bubble stabilization techniques [17,18,34] may have difficulty at a segment length ratio of 1/99 when a crack passes near the base of an element, since the effect of the bubble gets "weaker" as the crack approaches an element boundary. In contrast, the proposed stabilization technique works very well irrespective of the position of the crack relative to element sides.

Results of the simulations for the unstructured meshes are shown in Figs. 10 and 11. For clarity in presentation, we only report the stabilized solutions in Fig. 10 since the unstabilized solutions exhibit nearly as violent (if not worse) an oscillation as those encountered using the structured Meshes 1 and 2. Solutions obtained from the stabilized Lagrange multipliers and penalty methods are nearly the same, except with the coarser Mesh 3 where the stabilized penalty solution did not resolve the smooth variation of contact pressure as accurately as the stabilized Lagrange multipliers solution.

Fig. 11 shows the contact pressure distribution as a function of stabilization parameter τ. Once again, the unstabilized Lagrange multipliers solution oscillates more wildly than the unstabilized penalty solution. However, the Lagrange multipliers formulation also tends to be more receptive to stabilization since it produces a smooth variation of contact pressure even with a very small value of τ. Furthermore, the stabilized Lagrange multipliers solutions stay essentially the same even when τ is increased by two orders of magnitude.

4.2. 3D frictionless contact

We consider a unit cube ($1.0\,\text{m} \times 1.0\,\text{m} \times 1.0\,\text{m}$) with a horizontal frictionless crack surface shown in Fig. 12. The solid material has Young's modulus $E = 10$ GPa and Poisson's ratio $\nu = 0.3$. The bottom and top boundaries of the cube are clamped and moved toward each other in the z-direction by 0.10 m to induce a vertical compression. We use a mesh consisting of 9261 nodes and 40,000 four-node tetrahedral elements. For this example, each tetrahedral element cut by the crack is subdivided into four or six tetrahedra for the numerical integration of the bulk variational equations [32]. The crack surface is then discretized naturally by sub-triangles. The contact integral is evaluated on these sub-triangles, and a standard 13-point Gauss integration on each sub-triangle is used to evaluate the contact integrals.

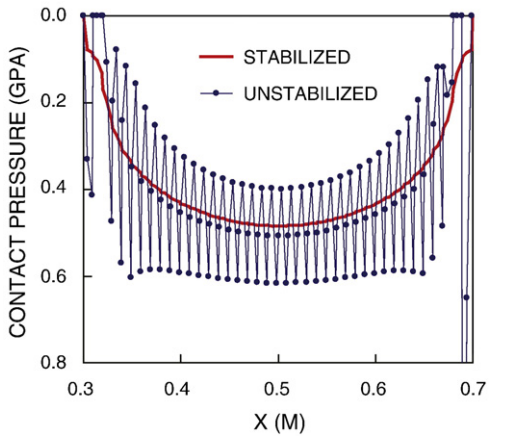

Fig. 23. Stabilized and unstabilized contact pressures on a diagonal frictional crack embedded in an elasto-plastic solid.

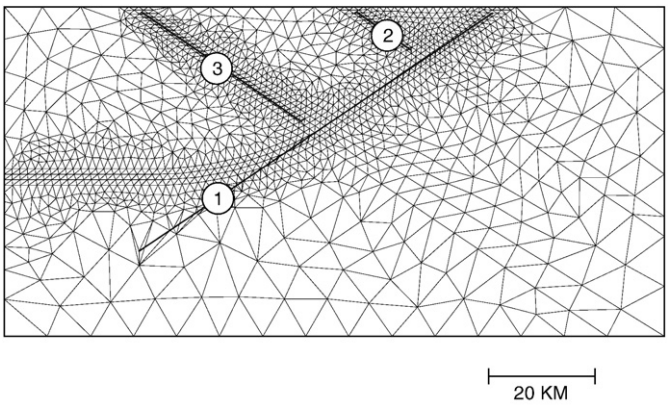

Fig. 24. FE mesh for elasto-plastic geological structure with three frictional faults.: the mesh has 1359 nodes and 2637 CST elements, and deforming in plane strain.

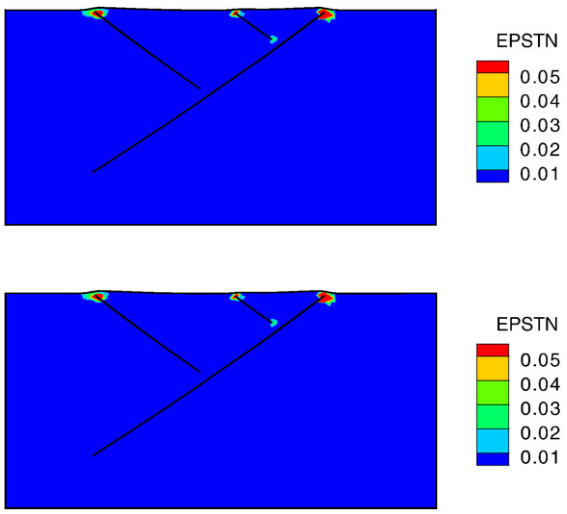

Fig. 25. Contours of plastic strain after a nominal horizontal contraction of 10 km from stabilized (top) and unstabilized (bottom) solutions.

The deformed mesh and displacement contour in the z-direction are shown in Fig. 12. Fig. 13 shows contours of the normal contact pressure generated by the unstabilized Lagrange multipliers and penalty methods. The unwanted oscillation in contact pressures is evident from the two solutions. Fig. 14, on the other hand, shows that the oscillation in contact pressures has been completely suppressed by the PPP stabilization technique (with $\tau = 1.0$).

4.3. Glued crack in plane strain

As noted in the Introduction, the performance of Nitsche's and bubble stabilization methods in frictional sliding contact has not yet been reported in the literature. Since these two methods have very similar variational forms, it suffices to compare the performance of the proposed PPP technique to that of Nitsche's method in an application where the latter method has already been used, namely, that of a glued crack, see [38]. The problem of a glued crack is, of course, quite trivial since it involves a simple stick mode. However, before a crack slides it must first satisfy a sliding condition, which is calculated using the traction stresses under a stick condition. Hence, if the stabilization technique is to be robust it must accommodate both the stick and slip conditions.

We consider a unit square (1 m × 1 m) cut by a horizontal crack passing through the center as shown in Fig. 15. We assume small deformation linear elasticity and plane strain loading, with Young's modulus $E = 10$ GPa and Poisson's ratio $\nu = 0.3$ for the bulk material. With the top and bottom surfaces clamped, the structure is then compressed and sheared by moving the top boundary downwards and to the right by 0.1 m in both directions, while keeping the crack in stick condition. We use the Lagrange multipliers and penalty methods ($\epsilon_N = 10^7$ GPa/m), with and without stabilization. Furthermore, we use Nitsche's method with $\alpha = 50$ GPa/m (see [38]) and PPP stabilization ($\tau = 1.0$).

Fig. 16 shows the normal and shear components of traction on the crack faces under a stick condition, with and without stabilization. It can be seen that both components of traction show instability in the form of oscillation, which has been alleviated significantly by Nitsche's and PPP stabilization approaches. However, whereas the normal contact pressures have been stabilized by both approaches to a point where no oscillation can be observed, the shear stresses calculated by Nitsche's method still exhibit some minor oscillation (a similar result has been reported in [38]). On the other hand, the PPP stabilization has suppressed any oscillation in both components of traction.

4.4. Glued crack in plane stress

In this section we focus on spatial convergence study by applying the stabilized algorithm to a problem where there is a known analytical solution, namely, that of an elastic cantilever beam (Young's modulus E and Poisson's ratio ν) bending in plane stress. The example follows [38] and is depicted in Fig. 17. The beam has a thickness of 1.0 (for simplicity we omit the units and assume that they have been used consistently throughout) and is subjected to a point load P at the free end. The analytical solutions for the model problem can be found in [45] and are summarized as follows.

The stresses are

$$\sigma_{xx} = -Pxy/I, \qquad \sigma_{yy} = 0, \qquad \sigma_{xy} = -P\left(c^2 - y^2\right)/2I, \tag{47}$$

where I is the moment of inertia and $2c$ is the depth of the cross-section. The displacements are

$$\begin{aligned} u_x &= -\frac{Px^2y}{2EI} - \frac{\nu Py^3}{6EI} + \frac{Py^3}{6\mu I} + ey \\ u_y &= \frac{\nu Pxy^2}{2EI} + \frac{Px^3}{6EI} + dx + h, \end{aligned} \tag{48}$$

where

$$e = \frac{PL^2}{2EI} + \frac{\nu Pc^2}{6EI} - \frac{Pc^2}{6\mu I}, \qquad d = -\frac{Pc^2}{2\mu I} - e, \qquad h = -\frac{PL^3}{6EI} - dL, \tag{49}$$

and $\mu = E/2(1+\nu)$ is the elastic shear modulus.

In the numerical simulations we used $P = 1.0$, $E = 1.0$, $\nu = 0.30$, $L = 16.0$ and $c = 2.0$. For reference, the glued interface (denoted by section A–A in Fig. 17) is located at $x = 8.0$. The penalty parameters are $\epsilon_N = \epsilon_T = 10^7$, and the stabilization parameters are $\tau = 1.0$ for the PPP stabilization and $\alpha = 50$ for the Nitsche stabilization.

We use five structured meshes for the spatial convergence study: the first mesh includes 90 nodes and 136 CST elements, the second includes 306 nodes and 528 CST elements, the third has 1122 nodes

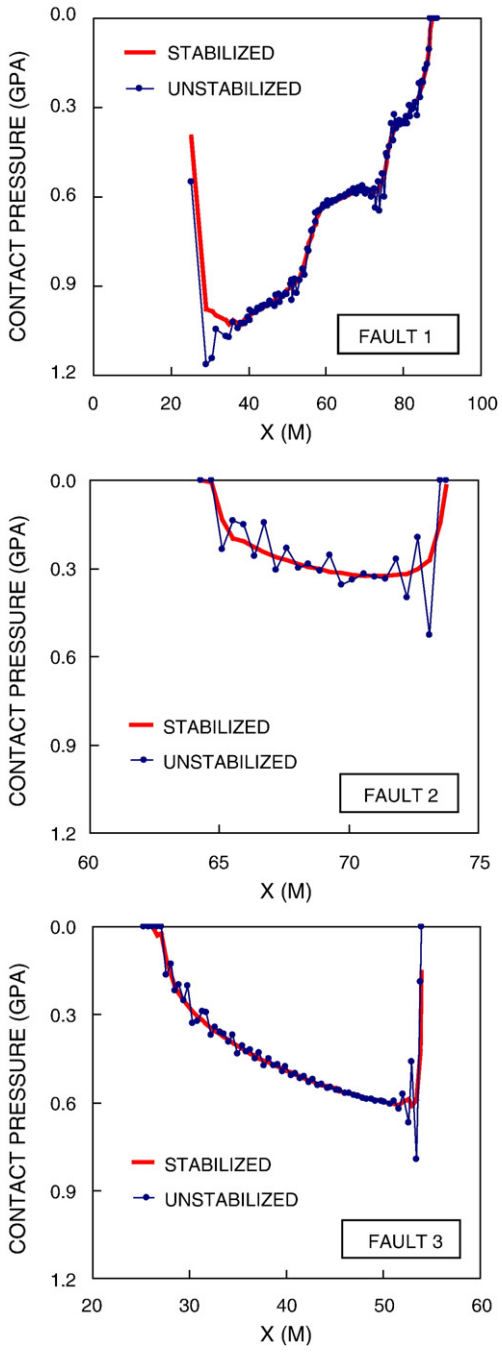

Fig. 26. Stabilized and unstabilized contact pressures on three frictional faults.

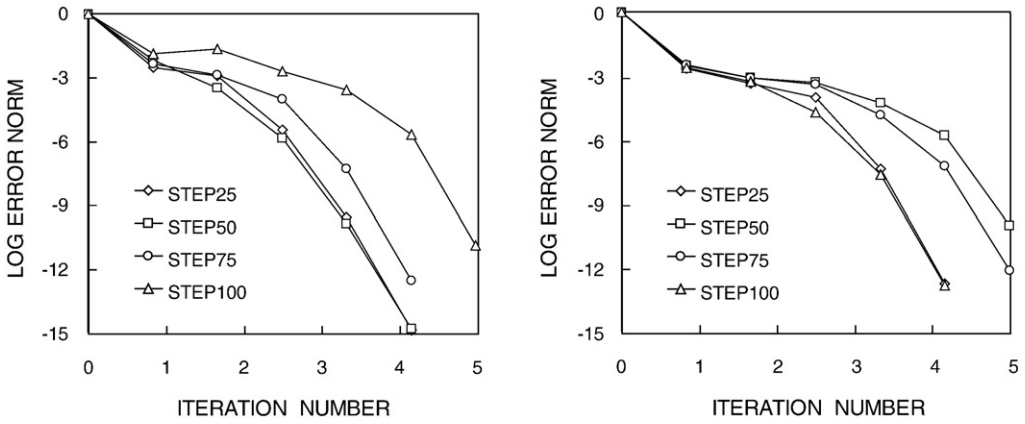

Fig. 27. Convergence profile of Newton iterations for elasto-plastic solid with diagonal crack: stabilized solution (left) and unstabilized solution (right).

and 2080 CST elements, the fourth includes 4290 nodes and 8256 CST elements, and the fifth mesh is defined by 16,770 nodes and 32,896 CST elements. Fig. 18 shows the L^2-norm of the errors in the bulk displacement field and demonstrates a quadratic convergence for the unstabilized and stabilized solutions. However, Fig. 19 shows that the unstabilized Lagrange multipliers and penalty methods cannot achieve convergence in the normal tractions. Quasi-linear convergence of tractions along the interface is achieved by the PPP and Nitsche's stabilization methods, but the PPP-stabilized Lagrange multipliers method has the steepest convergence rate in both the tangential and normal tractions. Nitsche's method and the PPP-stabilized penalty method exhibit approximately the same convergence rate, represented by the slopes of the error curves, but in general Nitsche's method produces larger errors in the tangential traction than the PPP-stabilized methods as the mesh is refined. From Fig. 20 we see that the tangential tractions are nearly the same as the exact solution for the PPP-stabilized solutions, but there are still oscillations in the tangential traction for Nitsche's solution. The latter result agrees with those reported in [38] for a similar problem.

4.5. Frictional contact

In this section we present two examples involving frictional cracks embedded in elasto-plastic domains. We consider the stabilized and unstabilized penalty formulations only as it is not trivial to implement the Lagrange multipliers method in the presence of frictional crack and bulk plasticity. In the first example we consider a diagonal crack embedded in the mesh shown in Fig. 21. The mesh, assumed clamped at both its top and bottom boundaries, is compressed vertically similar to the loading conditions considered in the examples of Section 4.1. This time we assume that the bulk material is elastic-perfectly plastic yielding according to the Drucker–Prager yield criterion with the following material parameters: Young's modulus of elasticity of $E=10$ GPa, Poisson's ratio 0.30, cohesion parameter $\alpha=0.17$ GPa, friction parameter $\beta=1.0$, and dilatancy parameter $b=0.8$ (see [8,28] for the physical meanings of these parameters). The coefficient of friction on the crack is assumed to be $\mu=0.10$, and the penalty parameters are $\epsilon_N=\epsilon_T=10^4$ GPa/m. All Gauss points are initially stress-free.

Fig. 22 shows nearly identical yield zones generated by the stabilized and unstabilized solutions. Both solutions suggest a propensity to develop wing cracks at the tips. Fig. 23 demonstrates once again the effectiveness of the proposed stabilization technique in completely eliminating oscillation in the normal contact pressure distribution. With the unstabilized formulation, the oscillation in contact pressure is most violent near the crack tips, but with the proposed stabilization technique this undesirable feature is nonexistent.

The second example deals with three frictional faults shown in Fig. 24. The loading is similar to the one considered in a previous publication that simulated the process of mountain-building [39]. Initial stress conditions are defined by the gravity load, and here we assume that the geologic structure has a mass density of $\rho=2.6$ T/m^3 (representative of rock) relevant for establishing the initial stress condition. Once again, we assume a non-associated Drucker–Prager model for the bulk material, with $E=10$ GPa, $\nu=0.25$, $\alpha=0.20$ GPa, $\beta=1.0$, and $b=0.8$; the coefficient of friction on the faults is 0.5, and the penalty parameters are $\epsilon_N=\epsilon_T=10^4$ GPa/m.

The yield zones calculated by the stabilized and unstabilized formulations are shown in Fig. 25, again showing no sign of numerical

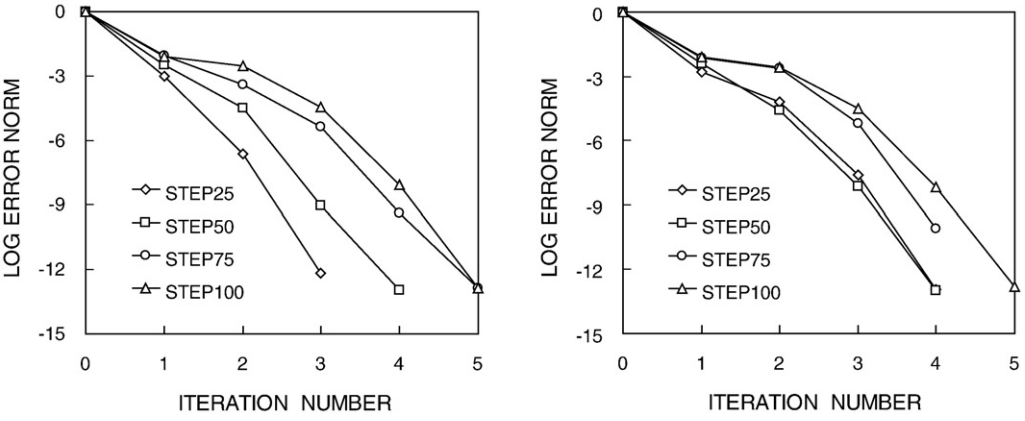

Fig. 28. Convergence profile of Newton iterations for elasto-plastic geologic structure with three faults: stabilized solution (left) and unstabilized solution (right).

instability. This is not true with the contact pressures, however, as Fig. 26 shows strong contact pressure oscillation (particularly near the fault tips) prevailing on all three faults, in the absence of stabilization. In contrast, the proposed stabilization technique completely eliminates this undesirable feature everywhere on all the three faults, once again demonstrating the efficacy of the algorithm.

Finally, we show the convergence profiles of Newton iterations in Figs. 27 and 28 for the two example problems considered. Because the stabilizing terms are linear functions of the contact pressures, they can easily be linearized, and the rate of convergence remains asymptotically quadratic.

5. Summary and conclusions

We have presented a stabilized extended FE formulation for frictional contact that minimizes, if not completely eliminates, the spurious oscillation of the contact pressure. The method is based on polynomial pressure projection (PPP) stabilization technique, which has been used successfully in previous work dealing with Stokes equation and classical solid-deformation/fluid-diffusion problems. Numerical results suggest that the technique is very effective in stabilizing frictional contact problems with structured and unstructured meshes, and with equal and unequal line segments. Furthermore, the technique has been implemented in the context of Lagrange multipliers and penalty methods. Specifically, the stabilized penalty formulation is unique in that we are not aware of any similar work in the literature in which the PPP approach has been formulated in the context of the penalty method. Both formulations (Lagrange multipliers and penalty) show optimal performance in stabilizing the contact pressure field. Further work is in progress to test the potential of the algorithm in the finite deformation regime.

Acknowledgments

This work is supported by the US Department of Energy grant no. DE-FG02-03ER15454, and National Science Foundation grant no. CMG-0417521 (Collaborations in Mathematical Geosciences). We are grateful to Dr. Joshua A. White for providing relevant references on the PPP technique. The first author acknowledges support from Stanford University through the Stanford Graduate Fellowship Program.

References

[1] D.N. Arnold, Mixed finite element methods for elliptic problems, Comput. Methods Appl. Mech. Engrg. 82 (1990) 8–300.
[2] E. Béchet, N. Moës, B. Wohlmuth, A stable Lagrange multiplier space for stiff interface conditions within the extended finite element method, Int. J. of Numer. Methods Engrg. 78 (2009) 931–954.
[3] T. Belytschko, N. Moës, S. Usui, C. Parimi, Arbitrary discontinuities in finite elements, Int. J. of Numer. Methods Engrg. 50 (2001) 993–1013.
[4] T. Belytschko, T. Black, Elastic crack growth in finite elements with minimal remeshing, Int. J. of Numer. Methods Engrg. 45 (1999) 601–620.
[5] G. Bilbie, C. Dascalu, R. Chambon, D. Caillerie, Micro-fracture instabilities in granular solids, Acta Geotech. 3 (2008) 25–35.
[6] P.B. Bochev, C.R. Dohrmann, M.D. Gunzburger, Stabilization of low-order mixed finite elements for the Stokes equations, SIAM J, Numer. Anal. 44 (1) (2006) 82–101.
[7] P.B. Bochev, C.R. Dohrmann, A computational study of stabilized, low-order C0 finite element approximations of Darcy equations, Comput. Mech. 38 (2006) 323–333.
[8] R.I. Borja, Assumed enhanced strain and the extended finite element methods: a unification of concepts, Comput. Methods Appl. Mech. Engrg. 197 (2008) 2789–2803.
[9] R.I. Borja, Conditions for instabilities in collapsible solids including volume implosion and compaction banding, Acta Geotech. 1 (2006) 107–122.
[10] R.I. Borja, Bifurcation of elastoplastic solids to shear band mode at finite strain, Comput. Methods Appl. Mech. Engrg. 191 (2002) 5287–5314.
[11] R.I. Borja, Finite element simulation of strain localization with large deformation: capturing strong discontinuity using a Petrov–Galerkin multiscale formulation, Comput. Methods Appl. Mech. Engrg. 191 (2002) 2949–2978.
[12] R.I. Borja, R.A. Regueiro, Strain localization of frictional materials exhibiting displacement jumps, Comput. Methods Appl. Mech. Engrg. 190 (2001) 2555–2580.
[13] R.I. Borja, A finite element model for strain localization analysis of strongly discontinuous fields based on standard Galerkin approximations, Comput. Methods Appl. Mech. Engrg. 190 (2000) 1529–1549.
[14] F. Brezzi, A discourse on the stability conditions for mixed finite element formulations, Comput. Methods Appl. Mech. Engrg. 82 (1990) 27–57.
[15] E. Burman, Pressure projection stabilizations for Galerkin approximations of Stokes' and Darcy's problem, Numer. Methods Partial Different. Equat. 24 (1) (2007) 127–143.
[16] C.R. Dohrmann, P.B. Bochev, A stabilized finite element method for the Stokes problem based on polynomial pressure projections, Int. J. Numer. Methods Fluids 46 (2004) 183–201.
[17] J. Dolbow, I. Harari, An efficient finite element method for embedded interface problems, Int. J. Numer. Meth. Engng. 78 (2009) 229–252.
[18] J.E. Dolbow, L.P. Franca, Residual-free bubbles for embedded Dirichlet problems, Comput. Methods Appl. Mech. Engrg. 197 (2008) 3751–3759.
[19] J. Dolbow, N. Moës, T. Belytschko, An extended finite element method for modeling crack growth with frictional contact, Comput. Methods Appl. Mech. Engrg. 190 (2001) 6825–6846.
[20] T. Elguedj, A. Gravouil, A. Combescure, A mixed augmented Lagrangian-extended finite element method for modelling elastic-plastic fatigue crack growth with unilateral contact, Int. J. of Numer. Methods Engrg. 71 (2007) 1569–1597.
[21] L.P. Franca, S.P. Oliveira, Pressure bubbles stabilization features in the Stokes problem, Comput. Methods Appl. Mech. Engrg. 192 (2003) 1929–1937.
[22] T.J.R. Hughes, Multiscale phenomena: Green's functions, the Dirichlet-to-Neumann formulation, subgrid scale models, bubbles and the origin of stabilized methods, Comput. Meth. Appl. Mech. Eng. 127 (1995) 387–401.
[23] H. Ji, J.E. Dolbow, On strategies for enforcing interfacial constraints and evaluating jump conditions with the extended finite element method, Int. J. of Numer. Methods Engrg. 61 (2004) 2508–2535.
[24] K.Y. Kim, J.E. Dolbow, T.A. Laursen, A mortared finite element method for frictional contact on arbitrary interfaces, Comput. Mech. 39 (2007) 223–235.
[25] T.A. Laursen, Computational Contact and Impact Mechanics: Fundamentals of Modeling Interfacial Phenomena in Nonlinear Finite Element Analysis, Springer-Verlag, Heidelberg, 2002.
[26] T.A. Laursen, J.C. Simo, A continuum-based finite element formulation for the implicit solution of multibody, large deformation frictional contact problems, Int. J. Numer. Methods Engrg. 36 (1993) 3451–3485.
[27] F. Liu, R.I. Borja, Finite deformation formulation for embedded frictional crack with the extended finite element method, Int. J. of Numer. Methods Engrg. 82 (2010) 773–804.
[28] F. Liu, R.I. Borja, A contact algorithm for frictional crack propagation with the extended finite element method, Int. J. of Numer. Methods Engrg. 76 (2008) 1489–1512.
[29] F. Liu, R.I. Borja, An extended finite element framework for slow-rate frictional faulting with bulk plasticity and variable friction, Int. J. Numer. Analyt. Methods Geomech. 33 (2009) 1535–1560.
[30] H. Magoariec, A. Danescu, B. Cambou, Nonlocal orientational distribution of contact forces in granular samples containing elongated particles, Acta Geotech. 3 (2008) 37–47.
[31] N. Moës, E. Béchet, M. Tourbier, Imposing Dirichlet boundary conditions in the extended finite element method, Int. J. of Numer. Methods Engrg. 67 (2006) 1641–1669.
[32] N. Moës, A. Gravouil, T. Belytschko, Non-planar 3D crack growth by the extended finite element and level sets—Part I: mechanical model, Int. J. of Numer. Methods Engrg. 53 (2002) 2549–2568.
[33] N. Moës, J. Dolbow, T. Belytschko, A finite element method for crack growth without remeshing, Int. J. of Numer. Methods Engrg. 46 (1999) 131–150.
[34] H.M. Mourad, J.E. Dolbow, I. Harari, A bubble-stabilized finite element method for Dirichlet constraints on embedded interfaces, Int. J. of Numer. Methods Engrg. 69 (2007) 772–793.
[35] I. Nistor, M.L.E. Guiton, P. Massin, N. Moës, S. Géniaut, An X-FEM approach for large sliding contact along discontinuities, Int. J. of Numer. Methods Engrg. 78 (2009) 1387–1512.
[36] P.J. Rabier, J.T. Oden, Solution to Signorini-like contact problems through interface models II. Existence and uniqueness theorems, Nonlin. Anal. 12 (1988) 1–17.
[37] P.J. Rabier, J.T. Oden, Solution to Signorini-like contact problems through interface models I. Preliminaries and formulation of a variational equality, Nonlin. Anal. 11 (1987) 1325–1350.
[38] J.D. Sanders, J.E. Dolbow, T.A. Laursen, On methods for stabilizing constraints over enriched interfaces in elasticity, Int. J. of Numer. Methods Engrg. 78 (2009) 1009–1036.
[39] P.F. Sanz, R.I. Borja, D.D. Pollard, Mechanical aspects of thrust faulting driven by far-field compression and their implications for fault geometry, Acta Geotech. 2 (2007) 17–31.
[40] D. Sheng, P. Wriggers, S.W. Sloan, Application of frictional contact in geotechnical engineering, Int. J. Geomech. 7 (2007) 176–185.
[41] L. Sibille, F.-V. Donzé, F. Nicot, B. Chareyre, D. Caillerie, From bifurcation to failure in a granular material: a DEM analysis, Acta Geotech. 3 (2008) 15–24.
[42] J.C. Simo, P. Wriggers, R.L. Taylor, A perturbed Lagrangian formulation for the finite element solution of contact problems, Comput. Methods Appl. Mech. Engrg. 50 (1985) 163–180.
[43] R. Stenberg, On some techniques for approximating boundary conditions in the finite element method, J. Comput. and Appl. Math. 63 (1995) 139–148.
[44] T.E. Tezduyar, Stabilized finite element formulations for incompressible flow computations, in: J.W. Huchinson, T.Y. Wu (Eds.), Advances in Applied Mechanics, vol. 28, Academic Press, 1998, pp. 1–44.

[45] S.P. Timoshenko, J.N. Goodier, Theory of Elasticity, McGraw-Hill Book Company, New York, 1971.
[46] A. Tordesillas, M. Muthuswamy, A thermomicromechanical approach to multi-scale continuum modeling of dense granular materials, Acta Geotech. 3 (2008) 225–240.
[47] J.A. White, R.I. Borja, Stabilized low-order finite elements for coupled solid-deformation/fluid-diffusion and their application to fault zone transients, Comput. Methods Appl. Mech. Engrg 197 (2008) 4353–4366.
[48] P. Wriggers, Computational Contact Mechanics, Wiley John & Sons, 2002.
[49] P. Wriggers, Finite element algorithms for contact problems, Arch. Comput. Methods Eng. 4 (1995) 1–49.
[50] P. Wriggers, T.V. Van, E. Stein, Finite-element-formulation of large deformation impact–contact-problems with friction, Comput. Struct. 37 (1990) 319–333.
[51] Z.H. Zhong, Finite Element Procedures for Contact–Impact Problems, Oxford University Press, 1993.